



RESEARCH ARTICLE OPEN ACCESS

A Novel Function of Na_v Channel β 3 Subunit in Endothelial Cell Alignment Through Autophagy Modulation

Léa Réthoré¹ | Anne-Laure Guihot¹ | Linda Grimaud¹ | Coralynne Proux¹ | Benjamin Barré^{2,3,4} | François Guillonnet^{3,4,5} | Catherine Guette^{3,4,5} | Alice Boissard^{3,4} | Cécile Henry^{3,4} | Jérôme Cayon⁶ | Rodolphe Perrot⁷ | Daniel Henrion¹ | Christian Legros¹  | Claire Legendre¹ 

¹INSERM, CNRS, MITOVASC, Equipe CarME, SFR ICAT, Univ Angers, Angers, France | ²Univ Angers, Angers, France | ³Institut de Cancérologie de l'Ouest (ICO), Angers, France | ⁴Prot'ICO (ICO Proteomic Core Facility), Angers, France | ⁵INSERM, CNRS, CRCI2NA, Nantes Université, Univ Angers, Angers, France | ⁶SFR ICAT, PACeM (Plateforme d'Analyse Cellulaire et Moléculaire), Univ Angers, Angers, France | ⁷SFR ICAT, SCIAM (Service Commun d'Imageries et d'Analyses Microscopiques), Univ Angers, Angers, France

Correspondence: Christian Legros (christian.legros@univ-angers.fr) | Claire Legendre (claire.legendre@univ-angers.fr)

Received: 11 July 2024 | **Revised:** 25 April 2025 | **Accepted:** 14 May 2025

Funding: This work was supported by the Fondation pour la Recherche Médicale (grant number FDT202204014720) and by the Fondation Banque Populaire Grand Ouest.

Keywords: autophagy | endothelial cell | mechanosignaling | Na_v β 3 | *SCN3B* | shear stress

ABSTRACT

Endothelial cells (EC) play a pivotal role in vascular homeostasis. By sensing shear stress generated by blood flow, EC endorse vasculoprotection through mechanotransduction signaling pathways. Various ion channels are involved in mechanosignaling, and here, we investigated the endothelial voltage-gated Na⁺ channels (Na_v channels), since their mechanosensitivity has been previously demonstrated in cardiomyocytes. First, we showed that EC from aorta (TeloHAEC) behave as EC from umbilical vein (HUVEC) under laminar shear stress (LSS). For both EC models, cell alignment and elongation occurred with the activation of the KLF2/KLF4 atheroprotective signaling pathways. We found that LSS decreased the expression of *SCN5A*, encoding Na_v1.5, while LSS increased that of *SCN3B*, encoding Na_v β 3. We demonstrated that the KLF4 transcription factor is involved in *SCN3B* expression under both static and LSS conditions. Interestingly, *SCN3B* silencing impaired EC alignment induced by LSS. The characterization of Na_v β 3 interactome by coimmunoprecipitation and proteomic analysis revealed that mTOR, implicated in autophagy, binds to Na_v β 3. This result was evidenced by the colocalization between Na_v β 3 and mTOR inside cells. Moreover, we showed that *SCN3B* silencing led to the decrease in LC3B expression and the number of LC3B positive autophagosomes. Furthermore, we showed that Na_v β 3 is retained within the cell and colocalized with LAMP1 and LC3B. Finally, we found that resveratrol, a stimulating-autophagy and vasculoprotective molecule, induced KLF4 together with Na_v β 3 expression. Altogether, our findings highlight a novel role of Na_v β 3 in endothelial function and cell alignment as an actor in shear stress vasculoprotective intracellular pathway through autophagy modulation.

Abbreviations: ANOVA, analysis of variance; B2M, Beta-2-Microglobulin; BSA, bovine serum albumin; Cq, cycle quantitative; DAPI, 4',6-diamidino-2-phenylindole; DDA, data-dependent acquisition; ddPCR, droplet digital polymerase chain reaction; DMEM, Dulbecco's modified Eagle medium; DRG, Dorsal Root Ganglion neurons; DTT, dithiothreitol; EBM-2, endothelial basal medium 2; EBM-MV2, endothelial basal medium from microvascular vessels; EC, endothelial cells; EDTA, ethylenediaminetetraacetic acid; EGM-2, endothelial growth medium 2; EGM-MV2, endothelial growth medium from microvascular vessels; eNOS, endothelial nitric oxide synthase; FDR, false discovery rate; FKBP12, FK506-binding protein 12; FT, flow through; GAPDH, glyceraldehyde-3-phosphate dehydrogenase; HAEC, human aortic endothelial cell; HSC70, heat shock cognate protein 70; HUVEC, human vein endothelial cell; Ig-CAM, immunoglobulin cellular adhesion molecule; IP, immunoprecipitation; KLF, krüppel-like transcription factor; LC3B or MAP1LC3B, microtubule-associated protein 1 light chain 3 beta M; LC-MS/MS, liquid chromatography coupled to tandem mass spectrometry; LSS, laminar shear stress; MMTS, S-Methyl methanethiosulfonate; mTOR, mammalian target of rapamycin; mTORC, mTOR complex; Na_v channels, voltage-gated Na⁺ Channels; PBS, phosphate-buffered saline; PCC, Pearson's correlation coefficient; PECAM1, platelet endothelial cell adhesion molecule; PEI, polyethylenimine; PFM, position frequency matrix; RSV, Resveratrol; TBP, tata-box protein; TRPV4, transient receptor potential vanilloid 4; TTX, tetrodotoxin; UBC, ubiquitin C.

This is an open access article under the terms of the [Creative Commons Attribution](https://creativecommons.org/licenses/by/4.0/) License, which permits use, distribution and reproduction in any medium, provided the original work is properly cited.

© 2025 The Author(s). *The FASEB Journal* published by Wiley Periodicals LLC on behalf of Federation of American Societies for Experimental Biology.

1 | Introduction

The endothelium is defined as a single layer of endothelial cells (EC) separating blood from the vessel wall. It plays a protective role in vascular homeostasis [1]. Indeed, the EC function allows the regulation of vasomotor tone in response to blood flow, as well as the preservation of blood vessel wall integrity and the regulation of angiogenesis [1]. Thus, endothelial function, via the vasculoprotective effects, preserves cardiovascular health, and endothelial dysfunction is a predictive factor for the occurrence of cardiovascular events including arterial hypertension and atherosclerosis. The endothelium is therefore a priority preventive and therapeutic target organ to reduce cardiovascular risk [2].

The key stimulus for EC function and vasculoprotection is the shear stress generated by laminar blood flow, which appears when the vessels are linear [3]. This laminar shear stress (LSS) ranges from 10 to 60 dyn/cm² in the arterial vascular network [4] and actively protects against vascular diseases through the activation of the atheroprotective molecular signaling pathways [5]. Among the flow-dependent transcription factors, Krüppel-like transcription factor (KLF) including KLF2 [6, 7] and KLF4 [8] are master regulators in the response of EC to LSS. KLF activation governs EC alignment in the direction of flow [9], associated with the structural reorganization of the actin cytoskeleton [9, 10]. KLF signaling pathway triggers also the expression of genes necessary for EC stability and quiescence, such as the endothelial nitric oxide synthase eNOS encoded by the *NOS3* gene, which promotes vasodilation and prevents inflammation [11].

Another mechanism involved in LSS-mediated endothelial vasculoprotection is autophagy. Autophagy refers to a set of pathways by which cytoplasmic content is sequestered in double-membrane vesicles called autophagosomes [12]. These autophagosomes are then subsequently degraded by fusion with lysosomes and generate autolysosomes, leading to the digestion and liberation of macromolecules and metabolites that can be re-used [12]. The autophagy process allows for cellular homeostasis maintenance [12] and participates in the vasculoprotection under LSS [13–15]. Autophagy also participates in the protective effects of vasculoprotective molecules such as resveratrol [16, 17]. Among the autophagic pathways described in EC, the serine/threonine kinase mTOR (mammalian target of rapamycin) is activated by low pathological shear stress, leading to inhibition of autophagy and subsequently to endothelial dysfunction [15]. The biogenesis of autophagosomes is governed by the last effector of autophagy, the microtubule-associated protein 1 light chain 3 beta MAP1LC3B, also called LC3B. Under LSS, the autophagy process is essential for cell alignment induced by LSS, and it prevents EC apoptosis, senescence, and inflammation [13–15] and regulates flow-mediated eNOS activation [16], linking cell recycling processes to the transduction of hemodynamic forces.

Indeed, LSS are sensed by specific membrane proteins that transduce mechanical forces into intracellular signals. These proteins are called mechanosensors or mechanotransducers, including mechanosensitive ion channels, such as the K⁺ channels Kir2.1, the nonselective cation channels transient receptor potential vanilloid 4, TRPV4, and Piezo1 [17]. The voltage-gated Na⁺ channels (Na_v channels) that are expressed in human vein endothelial cell HUVEC [20] modulate ERK signaling upon LSS in vitro [21]. Our

recent data have demonstrated that Na_v channels are involved in shear stress mechanosignaling, since the selective potent inhibitor of Na_v channels, tetrodotoxin (TTX), potentiates flow-mediated dilation response in resistance arteries [22].

Na_v channels are composed of two subunits, an α -subunit that forms a Na⁺ selective pore and an auxiliary β -subunit, belonging to the immunoglobulin cellular adhesion molecule Ig-CAM family, as chaperone and gating regulator [21]. In the mammal genome, nine genes (*SCN1-5A* and *SCN8-11A*) encode as many as Na_v channel α -subunit isoforms (Na_v1.1 to Na_v1.9) and four genes (*SCN1B* to *SCN4B*) encode Na_v channel β -subunit isoforms (Na_v β 1 to Na_v β 4, and also Na_v β 1B isoform resulting from alternative splicing of *SCN1B*) [22]. These ion channels are key components of membrane excitability and are mainly expressed in neurons, myocytes, and cardiomyocytes, allowing action potential generation and propagation [23]. However, for the past 2 decades, noncanonical roles of both α - and β -subunit isoforms of Na_v channels have emerged [24], such as phagocytosis [25] and migration and proliferation in cancer cells [26]. Mechanosensitivity of Na_v channels has been clearly demonstrated in cardiomyocytes and intestinal cells [27–31], through an electrical-contraction coupling mechanism, mediated by both Na_v β 1 and Na_v β 3 subunits [28].

Here, we aimed to better understand the role of Na_v channels in LSS. By investigating the expression of Na_v channels in EC submitted in vitro to LSS, we focused our attention on Na_v β 3, encoded by the *SCN3B* gene, in two human EC models, one obtained from umbilical vein (HUVEC), and the other from the aorta (TeloHAEC). We examined the correlation between *SCN3B* expression and cell alignment. Notably, we studied the relationship between *SCN3B* expression and KLF4, a vasculoprotective transcription factor, and the effects of *SCN3B* silencing on mTOR and LC3B expression, which govern autophagosome formation. Furthermore, we investigated in which intracellular compartments Na_v β 3 is expressed, in comparison with LAMP1, LC3B, and mTOR, to further address its role in autophagy. In addition, we explored the effect of resveratrol, a vasculoprotective molecule, on Na_v β 3 expression.

2 | Materials and Methods

2.1 | Chemical Reagents

All reagents and solvents were obtained from Sigma-Aldrich Merck (Saint-Louis, MO, USA) or Thermo Fisher Scientific (Waltham, MA, USA) except RapiGest SF Surfactant, which was obtained from Waters Corporation (186001861, Milford, MA, USA), and resveratrol (RSV) from Abcam (Cambridge, UK).

2.2 | Cell Lines and Treatments

Human umbilical vein endothelial cells (HUVEC) obtained from PromoCell (C-12203; Heidelberg Germany) were cultured from passage 2 until passage 5 at 37°C with 5% CO₂ in endothelial basal medium 2 (EBM-2; C-22211; PromoCell) supplemented with the SupplementMix (C-39216; PromoCell) called endothelial growth medium 2 (EGM-2). Human aortic endothelial cells

(TeloHAEC) (CRL-4052; LGC Standards, Molsheim, France) were cultured from passage 2 until passage 25 at 37°C with 5% CO₂ in endothelial basal medium from microvascular vessels (EBM-MV2; C-22221; PromoCell) supplemented with the SupplementMix (C-39226; PromoCell) called endothelial growth medium 2 from microvascular vessels (EGM-MV2). HUVEC and TeloHAEC were routinely cultivated in Flask T175 in EGM-2 or EGM-MV2 medium, respectively, and when 80% confluence was reached, split in a ratio of 1/5 (HUVEC) or 1/10 (TeloHAEC) in a new Flask T175 using the DetachKit (C-41210; PromoCell). COS-7 cells were cultivated in a Dulbecco's modified Eagle medium (DMEM)/F12 medium (P04-41550, Lonza, Basel, Switzerland) supplemented with 10% fetal bovine serum (Lonza), 1 mM L-glutamine, 1 mM of penicillin/streptomycin, and 1 mM of pyruvate in an incubator with 5% CO₂ at 37°C. COS-7 cells were routinely cultivated in Flask T75, and when 80% confluence was reached, split in a ratio of 1/10 in a new Flask T75. For resveratrol (RSV) treatment, HUVEC or TeloHAEC were plated at 80% confluence in 6-well plates and incubated the next day with 100 μM of RSV for 48 h in EGM-2 or EGM-MV2 using RSV solution stock of 100 mM freshly dissolved in DMSO. Control cells (CTL) were treated with 0.1% of DMSO.

2.3 | In Vitro Shear Stress Procedure

EC were seeded at 90% confluence (350 000 cells) onto μ-slides 0.4 or 0.8 Luer (80176; Ibidi GmbH, Munich, Germany) 24 h before shear stress experiments. The μ-slides were then connected to the Ibidi pump system (10902) with a perfusion set of 15 cm, inner diameter 1.6 mm (10962) according to the Ibidi manufacturer's instructions (AN 13: HUVECs under Perfusion). The slides were incubated at 37°C with 5% CO₂. Cells were exposed to a laminar unilateral shear stress (LSS) of 20 dyn/cm², with these flow parameters: 31.9 mbar pressure, 21.7 mL/min flow rate, 0.007 dyn × s/cm² viscosity for 24 h or 4 days. Static condition corresponded to cells cultivated onto Ibidi μ-slides 0.4 Luer without shear stress application. For this static condition, cell medium was changed every day.

2.4 | Cell Alignment and Elongation Quantifications

Cell alignment was assessed using the local gradient orientation method with the directionality plugins in ImageJ—Fiji software. Cell alignment is determined using the angle formed between the orientation vector of the flow direction (corresponding to an angle value of 0°) and the main axis of cells, called cell orientation in degree. The distribution of cells within each angle value (cell orientation in degree) is given as the cell amount value in arbitrary units. Histograms represent the quantity of cell alignment (in arbitrary unit) between the angle values of −5° to +5° to quantify all cells aligned to the flow direction.

Quantification of cell length and width giving the elongation factor (cell length along flow direction divided by cell width) was performed with ImageJ software, where for each technical replicate, 15 cells per field were counted for each culture condition (static or LSS).

2.5 | SiRNA or Plasmid Transfection

TeloHAEC were transfected with a custom *KLF4* SiRNA Oligo Duplex sequence called SiRNA *KLF4* or SiKLF4 (AGAUAAGCAAGAGGCGGU)(UU)—Eurofins Genomics, Ebersberg, Germany—or with *SCN3B* siRNA Oligo Duplex sequence (Locus ID 55800—SR310954) called SiRNA *SCN3B* or SiSCN3B (CCUAGUCACUGCAAUGUAUCUGAA—OriGene, Rockville, MD, USA) or with a universal scrambled negative control SiRNA duplex (AGGUAGUGUAAUCGCCUUG(UU)—OriGene, Rockville, MD, USA) called SiRNA CTL or SiCTL, using Lipofectamine RNAiMAX Reagent (Cat No. 13778-150, Invitrogen Life technologies, Thermo Fisher Scientific). Briefly, TeloHAEC were seeded at a density of 500 000 cells/well in a six-well plate. The day after, cells were transfected with a mix of 1:1 v/v lipofectamine: SiRNA (10 nM final) for 24 h. Cells were then trypsinized and seeded at 90% confluence (350 000 cells) onto μ-slides 0.4 Luer 24 h before the shear stress experiment for 24 h.

The expression plasmid, pMyc-SCN3B containing the ORF of *SCN3B* with a sequence encoding Myc tag (10 amino acid EQKLISEEDL) was used in this study (pCMV3-SP-N-Myc-SCN3B, Cat No. HG13897-NM, Sino Biological Europe, Düsseldorf, Germany). The vector pCTL served as the negative control vector (pCMV3-SP-N-Myc from Sino Biological Europe). TeloHAEC were transfected using Lipofectamine 2000 Reagent (Invitrogen Life technologies), whereas COS-7 cells were reverse transfected using Polyethylenimine (PEI, Cat No. 23966, Polysciences) according to the manufacturer's instructions. Cells were transfected with 1 μg of plasmid per 100 000 cells (TeloHAEC) or 300 000 cells (COS-7). TeloHAEC were also transfected with pPB[Exp]-EGFP/Puro-CMV>hKLF4 (NM_001314052.2), pKLF4 plasmid, (VectorBuilder, Neu-Isenburg, Germany) using Lipofectamine LTX with Plus Reagent (Invitrogen Life technologies) with 1 μg of plasmid per 100 000 cells for 24 h. The vector (pPB[Exp]-EGFP/Puro-CAG>ORF Stuffer, Cat No. VB010000-9294rpr, VectorBuilder) was used as the negative control.

2.6 | Reverse Transcription (RT) and Real-Time Quantitative Polymerase Chain Reaction (RT-qPCR)

After treatments, cells were washed with ice-cold PBS, and total RNA was extracted using the RNeasy micro kit (Qiagen, Courtaboeuf, France) according to the manufacturer's instructions. In total, 500 ng to 1 μg of total RNA was processed for cDNA synthesis using random hexamers and the QuantiTect Reverse Transcription kit (Qiagen). PCR assays were assessed on a LightCycler 480 Instrument II (Roche, Meylan, France) using Sybr Select Master Mix (Applied Biosystems, Thermo Fisher Scientific) or Power Sybr Select Master Mix and 10 ng of cDNA in duplicate, and gene-specific primers (Table S1) previously designed using the PrimerQuest Tool on Integrated DNA Technologies (IDT) and validated by testing PCR efficiency using a standard curve as per MIQE guidelines [32]. Amplification specificity was confirmed by one peak-melting curve at the end of the amplification process. Relative quantification of gene expression was normalized to the mean of the expression of two validated housekeeping genes TBP (Tata-box protein) and/or

UBC (Ubiquitin C) and/or B2M (Beta-2-Microglobulin) and by using the $2^{-\Delta Cq}$ or $2^{-\Delta\Delta Cq}$ method, where Cq is the Cycle quantitative [33].

2.7 | Droplet Digital Polymerase Chain Reaction (ddPCR)

The ddPCR experiments were performed using the QX200 ddPCR System (BioRad, Hercules, CA, USA), using 20 ng of cDNA normalized in quantity during the RT step. No-template controls and positive controls (i.e., HEK293 transfected with pMyc-SCN3B) were also tested. All samples were tested in duplicate. Each reaction was set up per the manufacturer's instructions in a 22 μ L sample volume containing 11 μ L of 2 \times ddPCR Evagreen supermix (Bio-Rad Laboratories Inc), 150 nM *SCN3B* specific forward primer AAGAGAGAGGAGGTGGAGGC and reverse primer GTGGCCATTCCGATACTCGT. Droplets were generated in a QX200 manual droplet generator according to the manufacturer's instructions, giving a final volume of 40 μ L. DNA amplification was carried out using the following PCR program: initial denaturation at 95°C for 5 min, amplification with 40 cycles at 95°C for 30 s and 60°C for 1 min followed by a final signal stabilization step at 4°C for 5 min and 90°C for 5 min (C1000 Touch thermal cycler; Bio-Rad Laboratories Inc). Finally, droplets were analyzed in a QX200 droplet reader with QuantaSoft software (Bio-Rad Laboratories Inc), and data analysis of ddPCR files, including Poisson distribution analysis, was performed with QuantaSoft Software Standard Edition (version 1.2, Bio-Rad Laboratories Inc). The threshold line differentiating positive from negative calls was determined automatically by the software and manually adjusted when necessary, using the signals in no-template controls and positive control, as a guide. The minimum number of accepted droplets for quantification was 8500. Quantitative ddPCR data were used to calculate *SCN3B* concentrations in copy/ μ L of sample, taking into consideration dilution factors.

2.8 | Western Blotting

After treatments, cells were washed with ice-cold PBS and lysed at 4°C in RIPA buffer (50 mM Tris-HCl, 150 mM NaCl, 12 mM sodium deoxycholate, 0.1% SDS, 1% Triton X-100, pH 8) supplemented with Halt Protease and Phosphatase Inhibitor Cocktail and EDTA (78444, Thermo Fisher Scientific). Cell lysates were centrifuged for 20 min at 14000 rpm at 4°C, and supernatants were collected. After protein quantification (Pierce BCA Protein Assay Kit, Cat No. 23235), 10 to 50 μ g of proteins were separated by 8% to 12% SDS-Polyacrylamide Gel Electrophoresis or 4%–20% precast polyacrylamide gel (Bio-Rad, Marnes-la-Coquette, France) and were transferred onto a nitrocellulose membrane 0.22 μ M (Thermo Fisher Scientific). The primary antibodies diluted in TBST 5% (w/v) BSA used were anti-eNOS/NOS Type III (1/500, mouse, 610297, BD Biosciences), anti-KLF2 (1/1000, rabbit, HPA055964, Atlas Antibodies), anti-KLF4 (1/1000, rabbit, 4038, Cell Signaling Technology), anti-Myc tag [9E10] (1/1000, mouse, ab32, Abcam, Cambridge, UK), anti-Na ν 1.5 (1/500, rabbit, ASC-005, Alomone Labs), anti-Na ν 1.6 (1/500, rabbit, ASC-009, Alomone labs), anti-Na ν 1.7 (1/500, mouse, 75-103,

NeuroMab), anti-Na ν β1 (1/1000, rabbit, 13950, Cell Signaling), anti-Na ν β3 (1/1000, rabbit, PA5-87803 or PA5-41403, Thermo Fisher Scientific or Ab4855, Abcam), anti-mTOR (1/1000, rabbit, 2972, Cell Signaling Technology), anti-P-mTOR 2448 (1/1000, rabbit, 2971, Cell Signaling Technology), anti-P-mTOR 2481 (1/1000, rabbit, 2974, Cell Signaling Technology), anti-LC3B (1/1000, rabbit, 3868, Cell Signaling Technology), and as loading controls: anti-GAPDH (1/2000, mouse, A5316, Sigma or 1/2000, rabbit, 2118, Cell Signaling Technology (14C10)), anti-β-actin (1/2000, mouse, A5316, Sigma), or anti-HSC70 (1/10000, mouse, sc-7298, Santa Cruz Biotechnology) were used as loading controls. Peroxidase-conjugated secondary antibodies (Goat anti-Mouse IgG, Cat No. 72-8062, and Goat anti-Rabbit IgG, Cat No. 72-8073, Tonbo Biosciences) and Clarity Western ECL Substrate (170-5061, Bio-Rad) or maximum sensitivity substrate SuperSignal West Femto (34095, Thermo Fisher Scientific) were used before visualization using a LAS-3000 imager (Fujifilm, Tokyo, Japan). The image acquisition was performed with Image Lab (Bio-Rad) and protein normalization and densitometry analysis were done by adjusting background and comparing the adjusted volume of each band of the interest protein to the adjusted volume of the band of the loading control (HSC70 or GAPDH). Data of densitometry analysis is available in Table S2.

2.9 | Immunofluorescence Staining and Colocalization Analysis

For immunofluorescence staining, TeloHAEC were cultivated onto μ -slides VI 0.4 Luer (80606; Ibbidi GmbH, Munich, Germany) previously coated with a gelatin-based coating solution 0.1% (P06-20410, PAN-Biotech GmbH, Aidenbach, Germany) before seeding at 40000 cells per channel. Cells were then subjected to SiRNA or plasmid transfection and cultivated under static or LSS conditions for 24 h. At the end of the experiments, cells were washed in PBS 1% at RT and fixed for 10 min with cold methanol 100% for LC3B staining or PFA 4% for the colocalization experiment and permeabilized for 10 min with 0.1% saponin in PBS (v/v) with 1% BSA, followed by 30 min blocking with 5% BSA, 0.01% saponin, and 100 mM glycine before probing with various primary antibodies at 4°C overnight. Antibodies used were as follows: anti-Na ν β3 (1/300, mouse, Alexa Fluor 488, S396-29 clone, NBP2-59318, Novus Biologicals, Toronto, Canada); anti-LC3B (1/100, rabbit, 2775, Cell Signaling Technology), anti-LAMP1 (1/200, rabbit, MA5-29385, Thermo Fisher Scientific) and anti-mTOR (1/100 rabbit, 2972, Cell Signaling Technology) in PBS/BSA 1%. After three washes in PBS/BSA 1%/saponin 0.01%, secondary antibodies Donkey antirabbit IgG (H + L) Alexa Fluor 568 (1/1000, A10042, Invitrogen, Thermo fisher Scientific) were then incubated for 45 min in PBS/BSA 1%. DAPI (10 μ g/mL, D9542, Sigma) was incubated for 10 min in PBS, and slides were mounted with Vectashield Mounting Medium (H-1000-10, Eurobio Scientific, Les Ulis, France). Staining of negative controls was performed under the same conditions with, respectively, Mouse IgG2b isotype control (133303), Alexa Fluor 488, (1/300, IC0041G, Novus Biologicals, Toronto, Canada), and donkey antirabbit IgG (H + L) Alexa Fluor 568.

For LC3B immunofluorescence staining, fluorescent staining was visualized using confocal microscopy with inverted microscope ECLIPSE 2000-E (Nikon, Champigny sur Marne, France)

using a 60× water immersion objective (Nikon Plan Apo 60 ON 1.2) and CoolSNAP_{HQ}² camera controlled by Metamorph software (Molecular Devices, San Jose, CA, USA). Z series size was 0.3 μm with the MS-2000 XYZ-LE Microscope Stage controlled. The excitation was performed at 408 nm for 500 ms or 561 nm for 2000 ms, and the emission filter used has band-pass respectively 460 ± 50 nm and 560 ± 50 nm.

For colocalization analysis, fluorescent staining was visualized using a Leica TCS SP8 AOBS confocal laser scanning microscope (Leica Microsystems, Wetzlar, Germany) equipped with a HC PL APO CS2 63X/ON 1.40 oil objective and gateable hybrid detectors (GaAsP). Images were acquired in the format 1024 × 1024 pixels, bit depth of 8, a scan speed of 400 Hz, and a X2 zoom using the LAS X software. Excitation was performed with a 488-nm Argon laser (40 mW), a 561-nm diode laser (20 mW) or a 633-nm He-Ne laser (10 mW). The bandpass for the detection of the emitted light was set, respectively, between 408 and 450 nm, 494 and 559 nm, and 564 and 630 nm. Z-series optical sections were collected with a step size of 0.3 μm using a Super Z Galvo Type H stage.

Quantification of LC3B puncta dot (count) and intensity fluorescence has been determined using ImageJ—Fiji. Six to ten fields by conditions (SiCTL or SiSCN3B) and by experiment have been analyzed, and three independent experiments have been performed. To quantify the colocalization between Navβ3 and LC3B (marker of autophagosomes) or LAMP1 (marker of for late endosomes and lysosomes) or mTOR, the Jacob plugin available in ImageJ—Fiji was used to calculate the Pearson correlation coefficient (PCC) to quantify the degree of colocalization between fluorophores (Alexa Fluor 488 for Navβ3 and Alexa Fluor 568 for LC3B or LAMP1 or mTOR). Five to fifteen cells by conditions (Static or LSS) and by experiment have been analyzed, and three independent experiments have been performed.

2.10 | Immunoprecipitation and Pull-Down Assay

After transfection with pMyc-SCN3B or pCTL vector for 24 h, TeloHAEC were washed with ice-cold PBS, collected, and lysed with IP lysis buffer (20 mM Tris pH 7.4, 150 mM NaCl, 1% Triton) containing Halt Protease and Phosphatase Inhibitor Cocktail and EDTA (78444, Thermo Fisher Scientific). Cell lysates were centrifuged for 20 min at 14000 rpm at 4°C, and supernatants, corresponding to input proteins, were collected for protein quantification (Pierce BCA Protein Assay Kit). For the immunocapture of Myc-Navβ3, 500 μg of protein extract were incubated with washed binding control magnetic agarose beads (Cat No. bmab-20, Chromotek) and rotated end-over-end for 1 h at 4°C. Then, this bead preparation was separated with a magnet until the supernatant was clear. This supernatant was incubated with washed Myc-Trap magnetic agarose beads (Cat No. ytma-10, Chromotek) overnight at 4°C. The next day, the Myc-Trap agarose beads were captured until the supernatant was clear. The supernatant was collected and named Flow Through (FT). Beads were washed twice with IP lysis buffer. The first wash, named Wash, was collected for checking the absence of Navβ3. After washing with IP lysis buffer without Triton, beads were boiled in NH₄CO₃ buffer

(50 mM pH 8) or with Laemmli buffer. The obtained supernatant (or elution named IP) was subjected to a western blot or mass spectrometry experiments. For the pulldown assay, COS-7 cells were transfected with pMyc-SCN3B plasmid or vector alone pCTL for 48 h. After collecting FT and Wash, 1 mg of freshly HUVEC whole protein lysate was incubated with magnetic beads for 1 h at 4°C in a rotating platform. Then, beads were washed twice with IP lysis buffer and once with IP lysis buffer without Triton. All protein samples (input, FT, wash, and IP) were analyzed by western blot.

2.11 | Sample Preparation and Proteomic Analysis

For MS/MS analysis, immunoprecipitates were resuspended in 200 μL of Rapigest SF (Waters), and dithiothreitol (DTT) was added to a final concentration of 5 mM (AppliChem, Darmstadt, Germany). Samples were incubated in a thermo shaker at 95°C for 1 h, and sonication was performed twice using an ultrasonic processor (130 W, 20 KHz) (Thermo Fisher Scientific). Subsequently, cysteine residues were alkylated by adding 200 mM S-Methyl methanethiosulfonate (MMTS) to a final concentration of 10 mM (incubated at 37°C for 10 min). Sequencing-grade trypsin was added in a ratio ≥ 2 μg per 100 μg of protein (incubated at 37°C overnight). The reaction was stopped with formic acid (9% final concentration) and incubated at 37°C for 1 h, and the acid-treated samples were centrifuged at 16000 g for 10 min. Salts were removed from the supernatant and collected in new reaction microtubes using self-packed C18 STAGE tips. Peptide concentrations were finally determined with the Micro BCA Protein Assay Kit (Thermo Fisher Scientific). 200 ng of each sample were analyzed by LC-MS/MS with a nanoHPLC UHPLC system (Bruker Daltonik GmbH, Billerica, MA, USA) with an Aurora series reversed-phase C18 column (25 cm × 75 μm i.d., 1.6 μm C18, IonOpticks) heated to 50°C and coupled to a TimsTOF Pro2 (Bruker Daltonik GmbH). A gradient of 2%–35% B, where mobile phase A was 0.1% formic acid in water and B was 0.1% formic acid in acetonitrile, was used for 1 h. The total run time, including a ramp up to 35%–95% B to clean the column, and prepare it for the next sample. The mass spectrometer was set to PASEF scan mode for DDA acquisition spanning 300–1250 m/z with 10 PASEF ramps. The TIMS settings were 100 ms ramp and accumulation time (100% duty cycle) and a ramp rate of 9.42 Hz; this resulted in 1.17 s of total cycle time. Linear precursor repetitions were set at a 20000 target intensity with a 2500 intensity threshold. Active exclusion was enabled with a 0.4 min release. The collision energy remained at default with a base of 1.6 1/K0 [Vs/cm²] set at 59 eV and 0.6 1/K0 [Vs/cm²] at 20 eV. Isolation widths were set at 2 m/z at < 700 m/z and 3 m/z at > 800 m/z. TIMS ranges were set initially from one range of 0.6–1.6 1/K0 [Vs/cm²] as seen in most published studies and further optimized and tested at a narrower range of 0.75–1.25 1/K0 [Vs/cm²]. Mass spectrometry data were analyzed with Protein Pilot software (v4.5, Sciex) using the following parameters: (1) search against a database composed of *Homo sapiens* from SwissProt (release on September 2022, with 26 610 reviewed entries); (2) MMTS as fixed modification; (3) trypsin digestion (with a miss cleavage factor of 0.75, Paragon Algorithm). An independent False Discovery Rate (FDR) analysis using the target-decoy approach provided by Protein Pilot was used to assess the quality of identifications. Positive identifications were considered when identified proteins and peptides reached a 5% local FDR.

2.12 | Statistical Analysis

All statistical analyses were realized using GraphPad Prism 7.02 (La Jolla, CA, USA). Normality of data distribution was assessed with the Shapiro–Wilk test (for the normal Gaussian distribution test), allowing for the choice of parametric or nonparametric statistical tests to analyze significance. Nonparametric unpaired *t*-test Mann–Whitney or one-sample *t* test and Wilcoxon test were used for comparison of two groups. Parametric or nonparametric one-way ANOVA was used for comparison of more than two groups. A difference with *p* value <0.05 was considered statistically significant (ns, nonsignificant, **p* <0.05, ***p* <0.01, ****p* <0.001, *****p* <0.0001). Data are mean ± SEM for at least three independent experiments.

3 | Results

3.1 | Effects of LSS on Cell Alignment and Elongation in TeloHAEC and HUVEC

In order to investigate the role of Na_v channels in LSS endothelial response, we used the TeloHAEC, which are a relevant model for in vitro study of LSS response as they originate from human aorta [32, 33]. Since there are no previous LSS experiments described to date, we first characterized the behavior of these cells in static condition and upon flow (20 dyn/cm²) in comparison to the well-known EC model, HUVEC [36] (Figure 1). As shown in cell images, TeloHAEC are mostly aligned and became more elongated in the flow direction after 24 and 96 h, as HUVEC (Figure 1A,B). The analysis of TeloHAEC phenotype under LSS showed a peak at 0°, reflecting that almost all cells exhibited an angle value of 0°, corresponding to cell alignment with the flow direction. In static condition, TeloHAEC did not show a particular distribution, rather a random orientation (Figure 1C). Histograms showed that the quantity of TeloHAEC aligned between the angle values of −5° to +5° was significantly higher under LSS condition than static conditions (*p* <0.05 at 24 h and *p* <0.01 at 96 h). HUVEC behaved similarly, as expected, but were less aligned than TeloHAEC after 24 h (Figure 1D). As such, we performed the next analysis after 96 h of LSS. The lengths of TeloHAEC significantly increased, from 75.9 ± 1.9 μm to 101.7 ± 3.8 μm after 96 h of LSS (*p* <0.001), whereas their widths decreased from 16.1 ± 0.5 μm to 10.9 ± 0.5 μm (*p* <0.001) (Figure 1E). As a consequence, the cell elongation factor (ratio of cell length/cell width) was significantly higher in TeloHAEC by 2-fold from 4.8 ± 0.16 μm to 9.6 ± 0.3 μm (*p* <0.001) (Figure 1E). Similar observations were made with HUVEC under LSS (Figure 1F). Taken together, these data showed that 96 h-LSS exposure at 20 dyn/cm² induced similar phenotypic modifications in both HUVEC and TeloHAEC, as cell alignment and elongation along the flow direction.

3.2 | Effects of LSS on Signaling Pathways in TeloHAEC and HUVEC

Next, we examined whether atheroprotective LSS (20 dyn/cm², 96 h) modified the expression of KLF2, KLF4, and eNOS at mRNA and protein levels, in TeloHAEC, as in HUVEC (Figure 2). While no change in *KLF2* mRNA expression was

observed in TeloHAEC (*p* = 0.68), KLF2 protein expression was significantly increased by LSS with fold change values of 6.7 ± 0.85 (*p* <0.05) (Figure 2A). The expression of KLF4 was increased at the levels of mRNA with a fold change of 5.5 ± 3.1 (*p* <0.05) and also at the protein level with a fold change of 5.5 ± 3.1 (*p* <0.05) (Figure 2B). No change in *NOS3* mRNA expression was found (*p* = 0.06), while a significant increase in protein expression (fold change values of 3.6 ± 0.7, *p* <0.01) occurred in TeloHAEC (Figure 2C). Similar observations were made in HUVEC (Figure 2A–C, right panel). Thus, the atheroprotective signaling pathway (KLF2/KLF4/eNOS) is efficiently activated by LSS in TeloHAEC, as in HUVEC.

3.3 | Effects of LSS on the Expression of Na_v Channel Subunits in TeloHAEC and HUVEC

To investigate whether Na_v channels contribute to mechanosensitive responses, we first characterized their expression in TeloHAEC and HUVEC in static and LSS conditions (Figure 3). *SCN5A*, *SCN8A*, and *SCN9A* transcripts were detected in both TeloHAEC and HUVEC in static condition (Cq values ~30 for 10 ng of cDNA except for *SCN8A* in HUVEC which give at Cq value of ~27) (Figure 3A). In contrast, *SCN1A*, *SCN2A*, *SCN3A*, *SCN4A*, *SCN10A*, and *SCN11A* transcripts were amplified at very low levels (Cq > 35 for 10 ng of cDNA), indicating that these genes were not expressed in TeloHAEC and HUVEC (Figure 3A). In these EC types, *SCN1B* and *SCN3B* cDNAs were detected with Cq values of ~27 and ~32 for 10 ng of cDNA respectively, while no expression was observed for *SCN2B* and *SCN4B* (Figure 3B). The expression of the corresponding Na_v channel subunits was validated at protein levels, that is, Na_v1.5, Na_v1.6, Na_vβ1, and Na_vβ3 types, except for Na_v1.7 (Figure 3C,D).

We next studied the impact of LSS on *SCN5A*, *SCN8A*, *SCN9A*, *SCN1B*, and *SCN3B* mRNA levels expressed endogenously in TeloHAEC and HUVEC. A significant downregulation of *SCN5A* expression was observed after 96 h of LSS with a 2.5-fold change in TeloHAEC (*p* <0.05) and a 4.7-fold change in HUVEC (*p* <0.01) (Figure 3E). The expression level of *SCN8A* mRNA did not change in TeloHAEC (*p* = 0.1) and also in HUVEC (*p* = 0.94) (Figure 3F). Surprisingly, the expression of *SCN9A* decreased in TeloHAEC (fold change of 0.6, *p* <0.05) and increased in HUVEC (fold change of 2.2, *p* <0.05) (Figure 3G). *SCN1B* expression did not significantly change in TeloHAEC (*p* = 0.17) and HUVEC (*p* = 0.19) (Figure 3H). Even more surprisingly, *SCN3B* expression level was increased by LSS by a 2.9-fold in TeloHAEC (*p* <0.05) and a 7.1-fold in HUVEC (*p* <0.01) (Figure 3I). At the protein level, we performed a western blot analysis only for Na_v1.5 and Na_vβ3, which showed the strongest variation in mRNA expression in the same direction. However, no change in Na_v1.5 protein level was observed after LSS in both EC types (Table S2). Concerning Na_vβ3, the 3-fold increase in protein expression level was found not significant in TeloHAEC (*p* = 0.1), while a significant 2.1-fold increase (*p* <0.05) was measured in HUVEC (Figure 3J). We assumed that the Na_vβ3 expression variation in TeloHAEC was not significant due to the weak expression of this protein in static conditions, as shown by the western blot (Figure 3J).

Taken together, the expression profile of Na_v channels is similar in TeloHAEC and HUVEC, at transcript (*SCN5A*, *SCN8A*, *SCN9A*, *SCN1B*, and *SCN3B*) and protein levels ($\text{Na}_v1.5$, $\text{Na}_v1.6$, $\text{Na}_v\beta1$, and $\text{Na}_v\beta3$), in static condition. Our data also show that

LSS modulates $\text{Na}_v1.5$ and $\text{Na}_v\beta3$ subunit expression. $\text{Na}_v1.5$ is downregulated by LSS at the transcript level in both TeloHAEC and HUVEC, but we were not able to validate this observation at the protein level. Interestingly, $\text{Na}_v\beta3$ expression was strongly

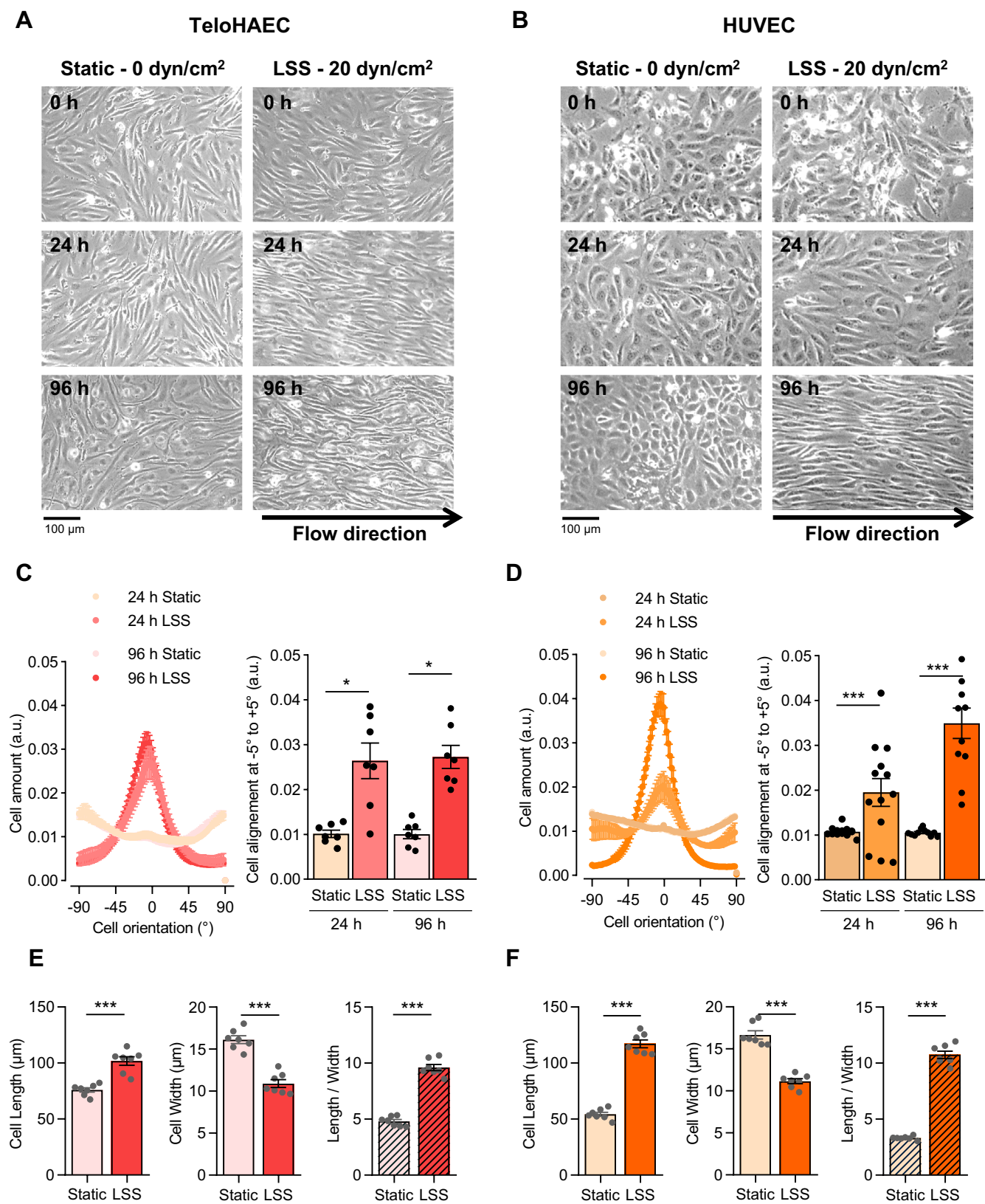


FIGURE 1 | Legend on next page.

FIGURE 1 | Phenotypic changes induced by LSS in TeloHAEC and HUVEC. Representative phase contrast microscopy images of TeloHAEC (A) and HUVEC (B) cultivated under static condition (Static, 0 dyn/cm²) or LSS (20 dyn/cm²) at different times (0, 24, and 96 h). TeloHAEC (C) and HUVEC (D) alignment quantification using local gradient orientation method with Fiji software at 24 and 96 h of LSS or under static condition. Cell amount is expressed over cell orientation in degree. A peak at angle value of 0° corresponds to a cell alignment with the flow direction. The histogram illustrates cell amount between angle values of -5° and +5°. Phenotypic modifications of TeloHAEC (E) and HUVEC (F) were assessed with the cell length (left panel) and width (middle panel), giving the elongation factor (Length/Width, right panel) after 96 h of LSS or of static culture. Values are mean ± SEM are shown ($n = 7-13$). Significance was analyzed using nonparametric Kruskal-Wallis (C, D) or Mann-Whitney (E, F) tests. * $p < 0.05$, *** $p < 0.001$.

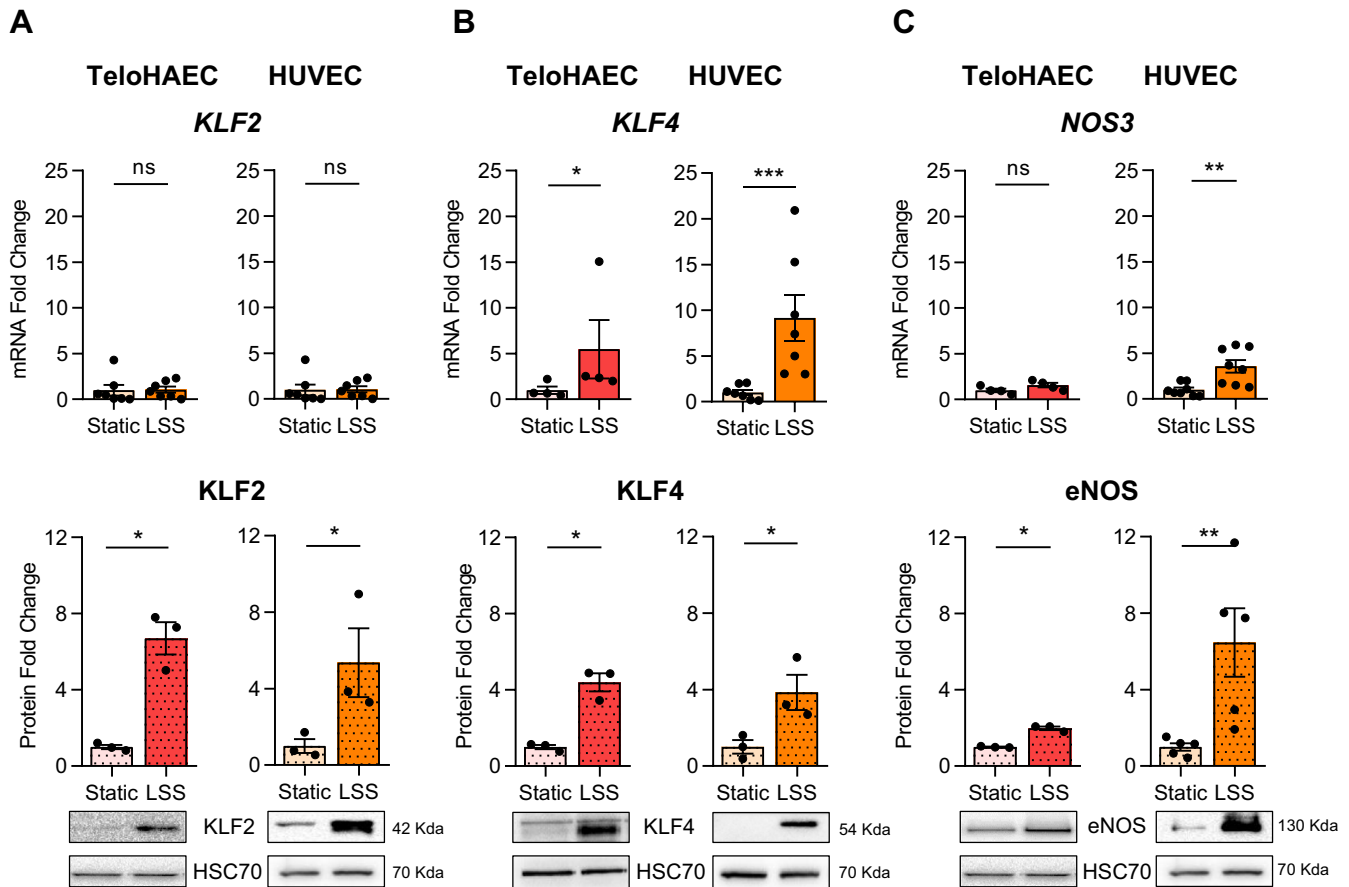


FIGURE 2 | Activation of the atheroprotective signaling pathway in TeloHAEC and HUVEC by LSS. The transcriptional and protein modification of *KLF2/KLF2*, *KLF4/KLF4*, and *NOS3/eNOS* expression induced by LSS (20 dyn/cm², 96 h) was measured in TeloHAEC and HUVEC, by RT-qPCR and western blotting, followed by densitometry analysis (A–C). The histogram bars illustrate the fold change values (mRNA and protein) as mean ± SEM ($n = 3-8$), compared to static condition, given the arbitrary value of 1 for RT-qPCR data or normalized to HSC70 (loading control protein) and compared to static condition, given the arbitrary value of 1 for western blotting. Nonparametric Mann-Whitney tests were performed. ns, nonsignificant, * $p < 0.05$, ** $p < 0.01$, *** $p < 0.001$.

upregulated by LSS in TeloHAEC and HUVEC. Thus, we focused our investigation on $\text{Na}_v\beta 3$ and its contribution in the endothelial mechanosignaling.

3.4 | Involvement of KLF4 Transcription Factor in *SCN3B* Expression Under Static and LSS Conditions in TeloHAEC

In order to understand how $\text{Na}_v\beta 3$ expression was increased by LSS in both EC types, we focused on one of the main signaling pathways activated by LSS, that is, KLF2/KLF4

transcription factors (Figure 4A). Since KLF4 acts upstream by regulating the expression of KLF2 [37], we first examined whether the *SCN3B* promoter contains a consensus-binding element for KLF4 respectively named MA0039.4 and MA0039.5 (Figure 4A). Among the 7 putative binding sites for KLF4 called S1 to S7 present in the Human *SCN3B* gene, the Jaspar analysis highlighted 4 putative binding sites for KLF4 before the transcription start site (TSS +1), thus belonging to the promoter region of *SCN3B* (Figure 4B and Table S3). To investigate the involvement of KLF4 in the regulation of *SCN3B* expression, TeloHAEC were transfected with pKLF4 and with the control vector (pCTL) (Figure 4C,D). After 24 h, a significant increase

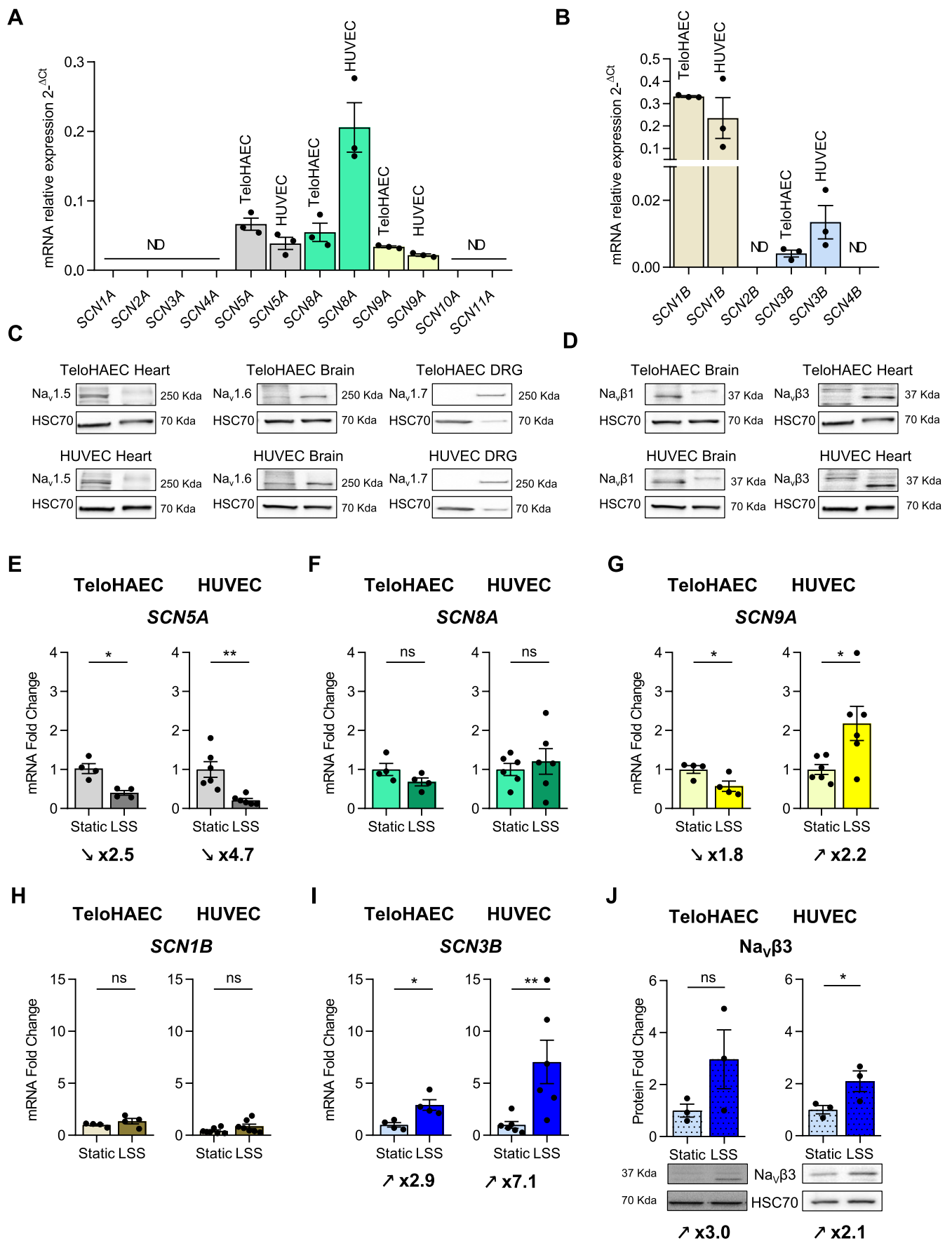


FIGURE 3 | Legend on next page.

FIGURE 3 | LSS modulates Na_v expression profiles in both TeloHAEC and HUVEC after 96 h of flow. mRNA expression profile of Na_v channel subunits (*SCN1A* to *SCN11A* and *SCN1B* to *SCN4B*) in TeloHAEC and HUVEC (A, B). The mRNA relative expression of Na_v channel subunits was determined by relative RT-qPCR. The data are mean of mRNA relative expression \pm SEM ($n=3$) with the $2^{-\Delta\text{Cq}}$ method. ND, not detected ($\text{Cq} > 35$). The protein expression of Na_v channel subunits detected at transcript level was evaluated by western blot in comparison to control tissues as mouse heart (for $\text{Na}_v1.5$ and $\text{Na}_v\beta3$), brain (for $\text{Na}_v1.6$ and $\text{Na}_v\beta1$) or Dorsal Root Ganglion neurons (DRG) (for $\text{Na}_v1.7$) (C, D). Fifty μg of cell protein extracts (TeloHAEC and HUVEC) and twenty μg of protein from control tissue (heart, brain and DRG) were loaded on 8% SDS-PAGE. HSC70 protein was used as a loading control (C, D). In TeloHAEC or HUVEC, $\text{Na}_v1.5$ and $\text{Na}_v\beta3$ share the same HSC70 loading control as well as $\text{Na}_v1.6$ and $\text{Na}_v\beta1$ since the protein samples immunoblotted with these antibodies ($\text{Na}_v1.5/\text{Na}_v\beta3$ and $\text{Na}_v1.6/\text{Na}_v\beta1$) are the same after cutting the nitrocellulose membrane. *SCN5A* (E), *SCN8A* (F) and *SCN9A* (G), *SCN1B* (H), *SCN3B* (I) mRNA expression and $\text{Na}_v\beta3$ protein expression (J) in LSS (20 dyn/cm^2 for 96 h) compared to static condition in TeloHAEC (left panel) and HUVEC (right panel). Values of fold change (mRNA and protein) are expressed as mean \pm SEM for at least 3 until 6 independent experiments and compared to static condition, given the arbitrary value of 1 using the $2^{-\Delta\Delta\text{Cq}}$ method for RT-qPCR experiments or normalized to HSC70 used as loading control protein and compared to static condition, given the arbitrary value of 1 for the densitometry analysis. Immunoblot representative images of $\text{Na}_v\beta3$ and HSC70 protein expression in TeloHAEC and HUVEC (J) cultivated under static or LSS (20 dyn/cm^2) condition for 96 h. Nonparametric Mann–Whitney tests were performed. ns, nonsignificant, * $p < 0.05$, ** $p < 0.01$.

in *KLF4* expression was observed with a fold change value of 58.2-fold for mRNA and 19.1-fold for protein levels ($p < 0.05$) (Figure 4C). Interestingly, this *KLF4* overexpression was associated with a significant increase in *SCN3B* mRNA level (1.80-fold, $p < 0.05$) and $\text{Na}_v\beta3$ protein level (1.86-fold, $p < 0.05$) (Figure 4D). Next, we decided to characterize the effects of *KLF4* silencing using siRNA on *SCN5A*, *SCN8A*, *SCN9A*, *SCN1B*, and *SCN3B* in TeloHAEC after LSS. The siRNA targeting *KLF4* (siKLF4) efficiently and strongly repressed *KLF4* expression in TeloHAEC after LSS with a fold change value of 14.3-fold ($p < 0.05$) (Figure 4E). While siKLF4 did not impact *SCN5A*, *SCN8A*, *SCN9A*, and *SCN1B* expression, it induced significantly a repression of *SCN3B* expression in TeloHAEC after LSS with a fold change value decrease of 3.3 ($p < 0.05$) (Figure 4F). Taken together, these data evidence that *KLF4* induction is involved in $\text{Na}_v\beta3$ expression under static conditions and triggered *SCN3B* expression in EC under LSS.

3.5 | Effect of siRNA Targeting *SCN3B* on Alignment and Morphology of TeloHAEC Under LSS

To establish the link between *SCN3B* and endothelial response to LSS, TeloHAEC were transfected with siRNA targeting *SCN3B* (SiSCN3B) prior to static or LSS conditions for phenotype characterization (Figure 5). Since the expression level of *SCN3B* was very low in conventional RT-qPCR (Cq values of ~ 32 for 10 ng of cDNA), we evaluated *SCN3B* expression using ddPCR technology, which is much more sensitive [38]. While *SCN3B* expression was significantly induced by LSS at 24 h with a fold change value of 1.5 ($p < 0.05$), the SiSCN3B efficiently decreased *SCN3B* expression significantly with a fold change of ~ 6.7 in both static ($p < 0.001$) and LSS ($p < 0.0001$) conditions (Figure 5A). The quantification of TeloHAEC alignment showed that SiSCN3B significantly decreased cell alignment in comparison with SiCTL condition under LSS ($p < 0.05$) (Figure 5B). Moreover, the cell dimension analysis showed that TeloHAEC width was significantly increased with SiSCN3B ($p < 0.05$) (Figure 5C). Thus, altogether these data show that *SCN3B* expression is correlated to the alignment and morphology of TeloHAEC after LSS.

3.6 | Identification of Protein Partners of $\text{Na}_v\beta3$ by Proteomic Analysis

Next, we aimed to identify $\text{Na}_v\beta3$ protein partners in EC by two distinct immunoprecipitation strategies using TeloHAEC and HUVEC (Figure 6). Thus, following transfection with the pMyc-*SCN3B* vector to express Myc- $\text{Na}_v\beta3$ in TeloHAEC (Figure 6A), the coimmunoprecipitated Myc- $\text{Na}_v\beta3$ proteins by anti-Myc-Trap magnetic agarose beads in TeloHAEC were directly subjected to LC-MS/MS and proteomic analysis (Figure 6A). COS-7 cells were also transfected with the pMyc-*SCN3B* vector, and anti-Myc-Trap magnetic agarose beads were used to immunocapture Myc- $\text{Na}_v\beta3$, followed by a pull-down assay using a whole HUVEC protein lysate (Figure 6B). Then, the coimmunoprecipitated Myc- $\text{Na}_v\beta3$ proteins were submitted to LC-MS/MS. Analysis with the DDA approach allowed the proteomic identification of 289 candidates as $\text{Na}_v\beta3$ partners in TeloHAEC and 510 in HUVEC (Figure 6C and Table S4). Our data allowed the identification of 65 novel *SCN3B* interactants, shared by TeloHAEC and HUVEC. 14 candidates in TeloHAEC and not in HUVEC are included in the *SCN3B* interactants list given by the GenBank database. 50 candidates in HUVEC and not in TeloHAEC are present in the GenBank *SCN3B* interactants list. Finally, 11 candidates identified in both TeloHAEC and HUVEC are also in the GenBank *SCN3B* interactants list (Figure 6C). A bioinformatic analysis of the functional roles was performed only on the 76 candidates shared in TeloHAEC and HUVEC (Table S4), using a gene ontology (GO)-term enrichment analysis using the ToppGene database. We focused on 4 GO-terms of two categories, that is, cellular component and biological process. Concerning the cellular component category, 30–40 proteins were distributed in the following GO-terms: organelle subcompartment, nuclear outer membrane–endoplasmic reticulum (ER) network, ER subcompartment, and ER membrane. Concerning the biological process category, 10–20 proteins are connected to the following functions: protein transport, establishment of protein localization, endomembrane system organization, and Golgi vesicle transport (Figure 6D).

Several interesting outputs of this analysis can be highlighted, but we choose to focus on mTOR, included in the 11 candidates

shared by both EC type and the GenBank *SCN3B* interactants list, because mTOR is present in all cellular component GO-terms and associated with autophagy, which is necessary for EC alignment under shear stress [15].

Thus, we decided to validate the interaction between $\text{Na}_v\beta 3$ and mTOR in EC by proceeding as described in Figure 6A,B,

and western blotting with mTOR antibody. The immunoprecipitation of Myc tag- $\text{Na}_v\beta 3$ in TeloHAEC allowed the immunodetection of mTOR (Figure 6E). The Myc tag- $\text{Na}_v\beta 3$ expressed in COS-7 also immunoprecipitated mTOR from whole HUVEC protein lysate (Figure 6F). mTOR was detected only in cells transfected with pMyc- $\text{Na}_v\beta 3$ in IP conditions and not in cells transfected with negative control plasmid (pCTL)

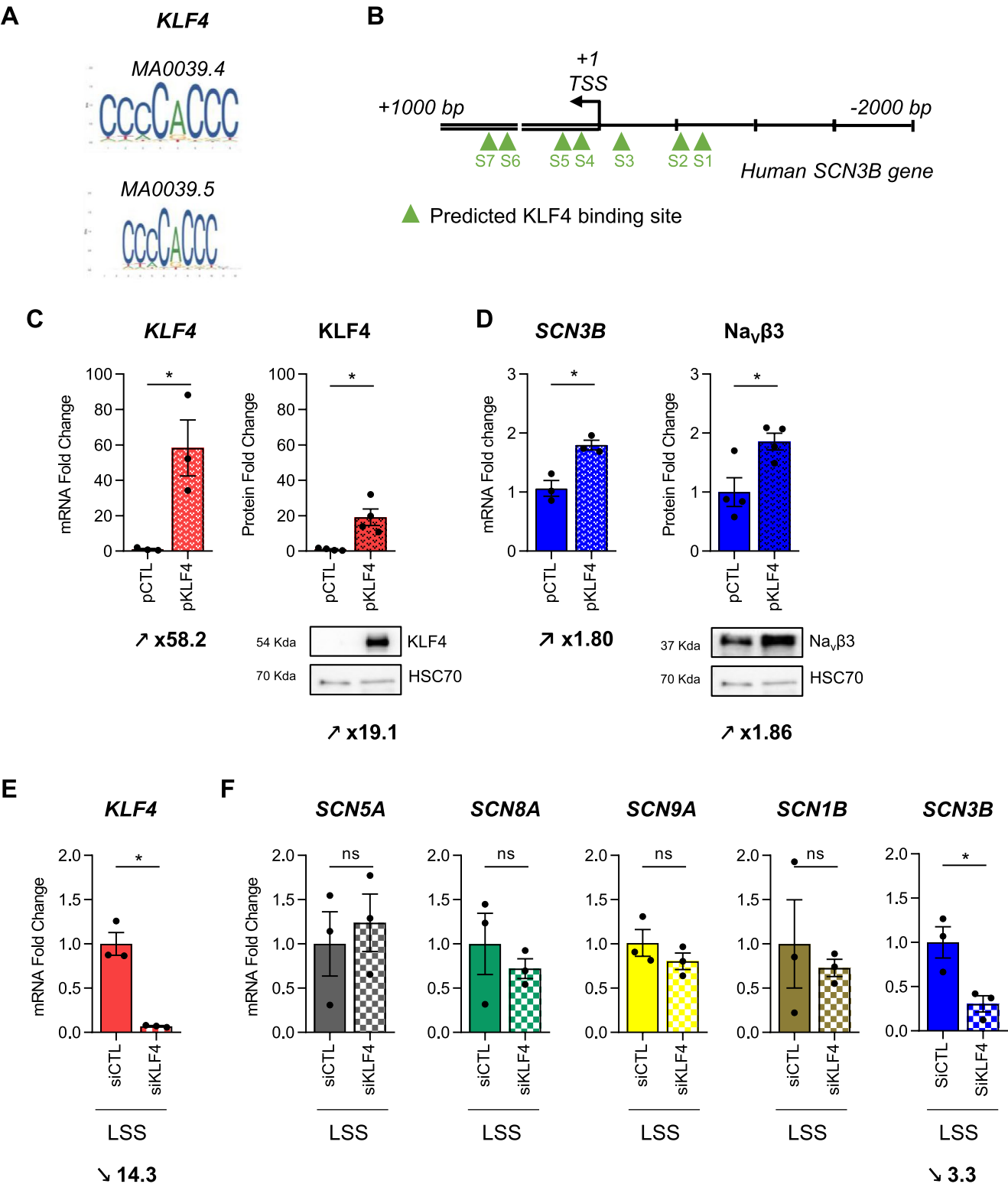


FIGURE 4 | Legend on next page.

FIGURE 4 | KLF4 is involved in *SCN3B* mRNA and protein expression in TeloHAEC. (A) Graphical representation of the KLF4 based on the position frequency matrix (PFM). The height of the column at each position is the information content (bit) and the individual base heights are in proportion to their frequencies. (B) Schematic representation of the location of the seven putative KLF4 (green triangles) DNA binding sites in human *SCN3B* promoter, with a score greater than 10.00, given by JASPAR analysis, named S1 to S7. (C, D) The effects of KLF4 overexpression using pKLF4 in comparison with empty vector (pCTL) were evaluated on KLF4 mRNA and protein (C) and *SCN3B* mRNA and Na_vβ3 protein (D) expression in TeloHAEC. (E, F) The effects of LSS (24 h at 20 dyn/cm²) on *KLF4* (E) and *SCN5A*, *SCN8A*, *SCN9A*, *SCN1B*, and *SCN3B* (F) expression were evaluated in TeloHAEC transfected with SiRNA Control (SiCTL) or SiRNA targeting KLF4 (SiKLF4). The histogram bars illustrate the fold change values (mRNA and protein) as mean ± SEM (*n* = 3–4), compared with pCTL or SiCTL, given the arbitrary value of 1 for RT-qPCR data using the 2^{-ΔΔC_q} method or normalized to HSC70 (loading control protein) and compared to pCTL, given the arbitrary value of 1 for western blotting. Values of mRNA fold change are expressed as mean ± SEM (*n* = 3) and compared to SiCTL condition, given the arbitrary value of 1. Significance was analyzed using nonparametric Mann–Whitney tests. ns, nonsignificant, **p* < 0.05.

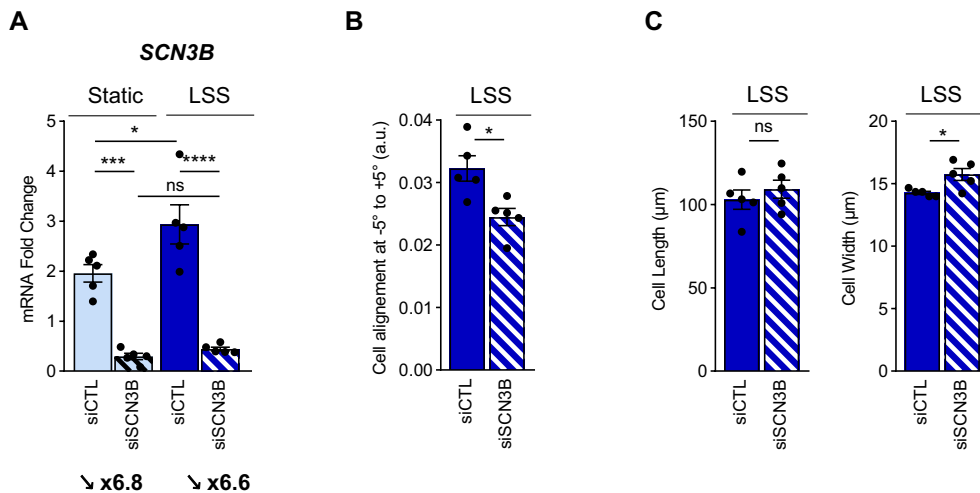


FIGURE 5 | SiRNA *SCN3B* decreased cell alignment and increased cell width after 24 h of LSS in TeloHAEC. (A) mRNA expression of *SCN3B* in TeloHAEC transfected with SiRNA Control (siRNA CTL) or SiRNA targeting *SCN3B* (SiRNA *SCN3B*) by ddPCR. Values of *SCN3B* mRNA fold change are expressed as mean of copy number of *SCN3B* per μL. (B) The histogram illustrates TeloHAEC amount between angle values of -5° and +5°, after transfection with SiRNA Control (siRNA CTL) or SiRNA targeting *SCN3B* (siRNA *SCN3B*). (C) Elongation of HUVEC was determined as the cell length along flow direction (left panel) divided by cell width (right panel). TeloHAEC were submitted to static or LSS (20 dyn/cm²) for 24 h. Values are mean ± SEM are shown (*n* = 5). Significance was analyzed using one-way ANOVA statistical analysis, followed by Tukey multiple comparisons test or nonparametric Mann–Whitney tests. ns, nonsignificant, **p* < 0.05, ****p* < 0.001, *****p* < 0.0001.

in TeloHAEC (Figure 6E). In HUVEC, mTOR was found in input (Inp), flow through (FT) in both conditions but only in IP conditions in cells transfected with pMyc-Na_vβ3 and not in cells transfected with negative control plasmid (pCTL) (Figure 6F).

As such, these data demonstrate that among the Na_vβ3 partners identified by the proteomic approach, mTOR interacts physically with Na_vβ3 in EC, suggesting the implication of Na_vβ3-mTOR-mediated autophagy signaling.

3.7 | Effect of *SCN3B* SiRNA on Autophagy Signaling Pathway in TeloHAEC Under LSS

Since Na_vβ3 interacts with mTOR, a master negative regulator of autophagy, and because autophagy is a crucial component for cell alignment upon LSS and endothelial function [13–16, 37], we then investigated the effects of SiSCN3B on the expression of the terminal effector of autophagy, LC3B, in TeloHAEC under static and LSS conditions. First, we observed that SiSCN3B did not modify the mTOR protein level nor the phosphorylation

status of mTOR associated with mTORC1 or mTORC2 complexes in static and LSS conditions (Figure 7A). These results are in accordance with the observation that, despite other partners of the mTOR complex (mTORC) being detected by LC-MS/MS in the immunocaptured Myc-Na_vβ3, these interactions have not been validated by subsequent western blot (data not shown). This concerned Raptor or mLST8 involved in the mTORC1 complex (Table S4) or Rictor involved in the mTORC2 complex.

Concerning LC3B expression under LSS and the impact of the SiRNA targeting *SCN3B* (Figure 7B), we found first that LSS led to a significant induction of *LC3B* mRNA with a fold change value of 1.6 in comparison with static condition (*p* < 0.05). Interestingly, SiSCN3B significantly decreased *LC3B* upregulation induced by LSS by 1.8-fold (*p* < 0.05). Concerning *LC3B* protein levels, both *LC3B*-I (cytosolic form) and *LC3B*-II (membrane bound form present in autophagosomes) were significantly increased by LSS (Figure 7C) with fold change values of 1.6 ± 0.3 for *LC3B*-I (*p* < 0.001) and 5.9 ± 1.5 (*p* < 0.01) for *LC3B*-II (Figure 7D). Interestingly, SiSCN3B induced a significant 2.9-fold and 2.6-fold decrease in *LC3B*-I protein expression respectively in both static and LSS conditions (*p* < 0.05, *p* < 0.01, respectively)

(Figure 7C,D). However, SiSCN3B did not impact LC3B-II protein expression ($p=0.99$) where expression was strongly induced by LSS with a fold change value of 5.9 (Figure 7C,D).

Interestingly, the repression of *SCN3B* expression under LSS by SiRNA silencing drastically dropped the number of

autophagosomes characterized by LC3B puncta or dots present inside the cells as well as LC3B fluorescence intensity, illustrated by immunofluorescence images of LC3B staining (Figure 7E). Indeed, the number of LC3B dots decreased by 1.7-fold in SiSCN3B treated cells ($p<0.05$) in comparison with SiCTL condition (Figure 7F, left panel) with a mean of 178 ± 43 puncta by

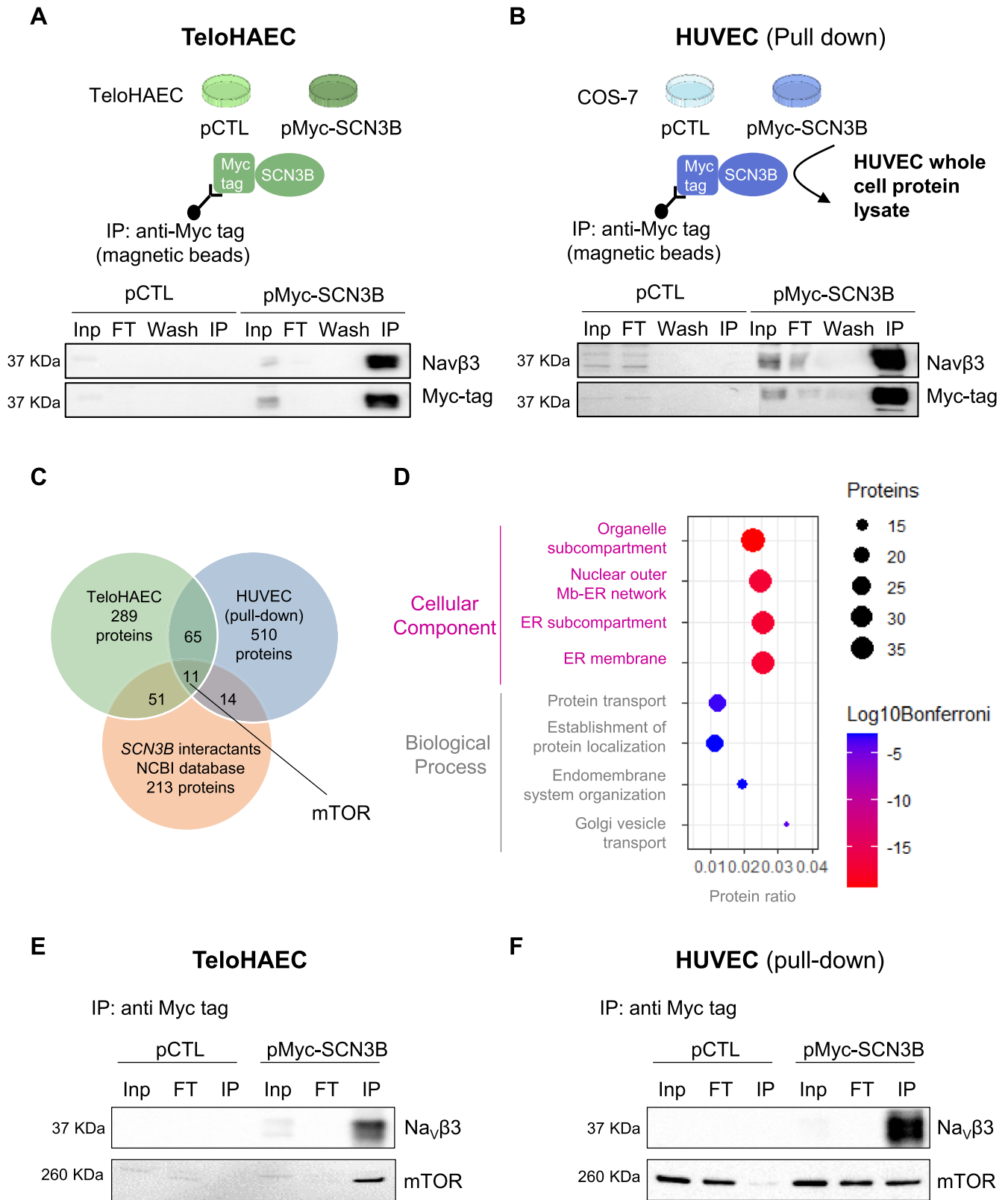


FIGURE 6 | Legend on next page.

FIGURE 6 | Identification of $\text{Na}_v\beta 3$ -interacting partners in TeloHAEC and HUVEC by proteomic analysis. (A, B) Schematic representation of the $\text{Na}_v\beta 3$ immunoprecipitation (IP) procedures. TeloHAEC (A) and COS-7 (B) were transfected with pMyc-SCN3B, and pCTL (negative control). (A) Myc tag- $\text{Na}_v\beta 3$ with its partners were coimmunoprecipitated using anti-Myc tag magnetic beads from TeloHAEC protein extracts. (B) Myc tag- $\text{Na}_v\beta 3$ from COS-7 protein extracts were first immunocaptured with anti-Myc tag magnetic beads and subjected to pull-down using HUVEC whole cell protein lysate. Below the schemes are shown representative control immunoblots ($n = 3$) with anti- $\text{Na}_v\beta 3$ (top blot) and anti-myc tag (bottom blot). Input (Inp) was the whole protein extract after cell transfection and the flow throw (FT) corresponded to the supernatant recuperated after immunocapturing with the anti-Myc tag magnetic beads. Wash and IP correspond to the washing step and a sample from the solution used to boil the beads (IP) to elute $\text{Na}_v\beta 3$ and its partners. IP from TeloHAEC and HUVEC were subjected to MS/MS analysis. (C) Venn Diagram indicating the number of $\text{Na}_v\beta 3$ interacting proteins identified in TeloHAEC and HUVEC after proteomic analysis. (D) Bubble plots of Gene ontology (GO)-term enrichment analysis of the 76 putative $\text{Na}_v\beta 3$ interactants. The four first GO-terms belonging to the biological process and cellular component categories are indicated on the left. Below the bubble chart, is shown the protein ratio (number of proteins in our dataset compared to number of proteins in annotation). The scale of the bubble plot size (black, upper right) reflects the number of proteins. The significance of the identification score is illustrated by a color intensity scale (Log10 Bonferroni, lower right). (E, F) Representative $\text{Na}_v\beta 3$ and mTOR immunoblots ($n = 3$) of immunoprecipitated $\text{Na}_v\beta 3$ with Myc tag antibody in TeloHAEC (E) and HUVEC (F).

field counted in SiCTL-treated cells in comparison with 99 ± 26 puncta in SiSCN3B-treated cells under LSS (Table S5). This diminution of puncta numbers was correlated to LC3B fluorescence intensity which decreased by 1.8-fold in SiSCN3B condition compared to SiCTL ($p < 0.05$) (Figure 7F, right panel). Taken together, our results show that SiRNA targeting *SCN3B* does not influence the protein level or phosphorylation status of mTOR but alters the increase of LC3B autophagosome puncta number and LC3B expression induced by LSS.

3.8 | Colocalization of $\text{Na}_v\beta 3$ With LC3B, LAMP1 and mTOR in TeloHAEC Under Static and LSS Conditions

Next, we investigated whether $\text{Na}_v\beta 3$ colocalizes with specific markers of organelles such as LC3B for autophagosomes or LAMP1 for late endosomes and lysosomes [40] (Figure 8). While a membrane distribution was expected, $\text{Na}_v\beta 3$ was immunolabeled in the nuclei and the cytosol. We did not observe clear $\text{Na}_v\beta 3$ immunolabeling at the plasma membrane, but rather a puncta labeling distribution (Figure 8). The immunofluorescence images illustrate a colocalization of $\text{Na}_v\beta 3$ with LAMP1, but not a clear colocalization with LC3B and mTOR (Figure 8A). Subsequent analysis of colocalization between $\text{Na}_v\beta 3$ and proteins of interest in TeloHAEC under static and LSS conditions was analyzed using the Pearson's correlation coefficient (PCC) which measures the pixel-by-pixel covariance in the signal levels of two images (Figure 8B). The colocalizations of $\text{Na}_v\beta 3$ with LC3B, LAMP1, and mTOR were evidenced by significant PCC values greater than 0 but below 1, encompassing between 0.28 and 0.47 (Table S6). Thus, we showed that $\text{Na}_v\beta 3$ colocalized with LAMP1 to a greater extent than LC3B, since PCC values for LAMP1 were significantly higher than those obtained for LC3B, with LAMP1 PCC values of 0.46 ± 0.02 under static condition ($p < 0.001$) and 0.47 ± 0.01 LSS condition ($p < 0.001$) (Figure 8B). No significant differences were observed between PCC values calculated for LC3B, LAMP1, and mTOR, respectively, in both static and LSS conditions. Altogether, our data show that the majority of $\text{Na}_v\beta 3$ is retained intracellularly, specifically within the late endosomes and lysosomes and to a lesser extent with autophagosomes, and interacts with mTOR similarly in static and LSS conditions.

3.9 | Effects of Resveratrol on SCN3B Expression in HUVEC and TeloHAEC

To support the idea that $\text{Na}_v\beta 3$ is involved in the autophagy process and vasculoprotection, EC were treated with resveratrol (RSV), which induces an atheroprotection [41] through the activation of KLF4 signaling [42] and autophagy [16, 17]. RSV exposition ($100 \mu\text{M}$ for 48 h) led to an increase in KLF4 expression with a 6.6-fold change in TeloHAEC ($p < 0.05$) and a 4.5-fold change in HUVEC ($p < 0.05$) (Figure 9A) together with the autophagic marker *LC3B* expression with a 2.4-fold change in TeloHAEC ($p < 0.05$) and a 1.7-fold change in HUVEC ($p < 0.05$) (Figure 9B). Interestingly, *KLF4* and *LC3B* induction mediated by RSV was correlated with a strong increase in *SCN3B* expression in TeloHAEC (fold change value of 5.4, $p < 0.05$) and a moderate but significant induction in HUVEC (fold change value of 1.9, $p < 0.05$) (Figure 9C). Induction of *SCN3B* seems to be specific to this gene family since *SCN1B* expression was not modulated by RSV in TeloHAEC (data not shown). The increase in KLF4, LC3B, and *SCN3B* by RSV was also observed at the protein level in TeloHAEC, where RSV induced an increase in KLF4, LC3B-II, and $\text{Na}_v\beta 3$ with fold change values of 3.5, 2.0, and 1.8, respectively (Figure 9D). Taken together, these data show that RSV-induced vasculoprotection and autophagy is associated with the activation of $\text{Na}_v\beta 3$ expression.

4 | Discussion

The main output of this study is that the auxiliary Na_v subunit, $\text{Na}_v\beta 3$ plays a role in cell alignment in response to physiological shear stress. Indeed, we showed that in TeloHAEC, $\text{Na}_v\beta 3$ is induced by KLF4, a key regulator of endothelial function and atheroprotective signaling pathway. Moreover, we demonstrated that $\text{Na}_v\beta 3$ is expressed intracellularly mainly inside lysosomes, contributes to the regulation of the autophagy pathway involved in cell alignment through its interaction with mTOR and the modulation of the number of autophagosomes formation. Thereby, $\text{Na}_v\beta 3$ is a novel actor in EC mechanosignaling in response to shear stress and might contribute to vasculoprotection.

Under a physiological LSS, EC change their phenotype, going from a so-called cobblestone shape to a more elongated shape

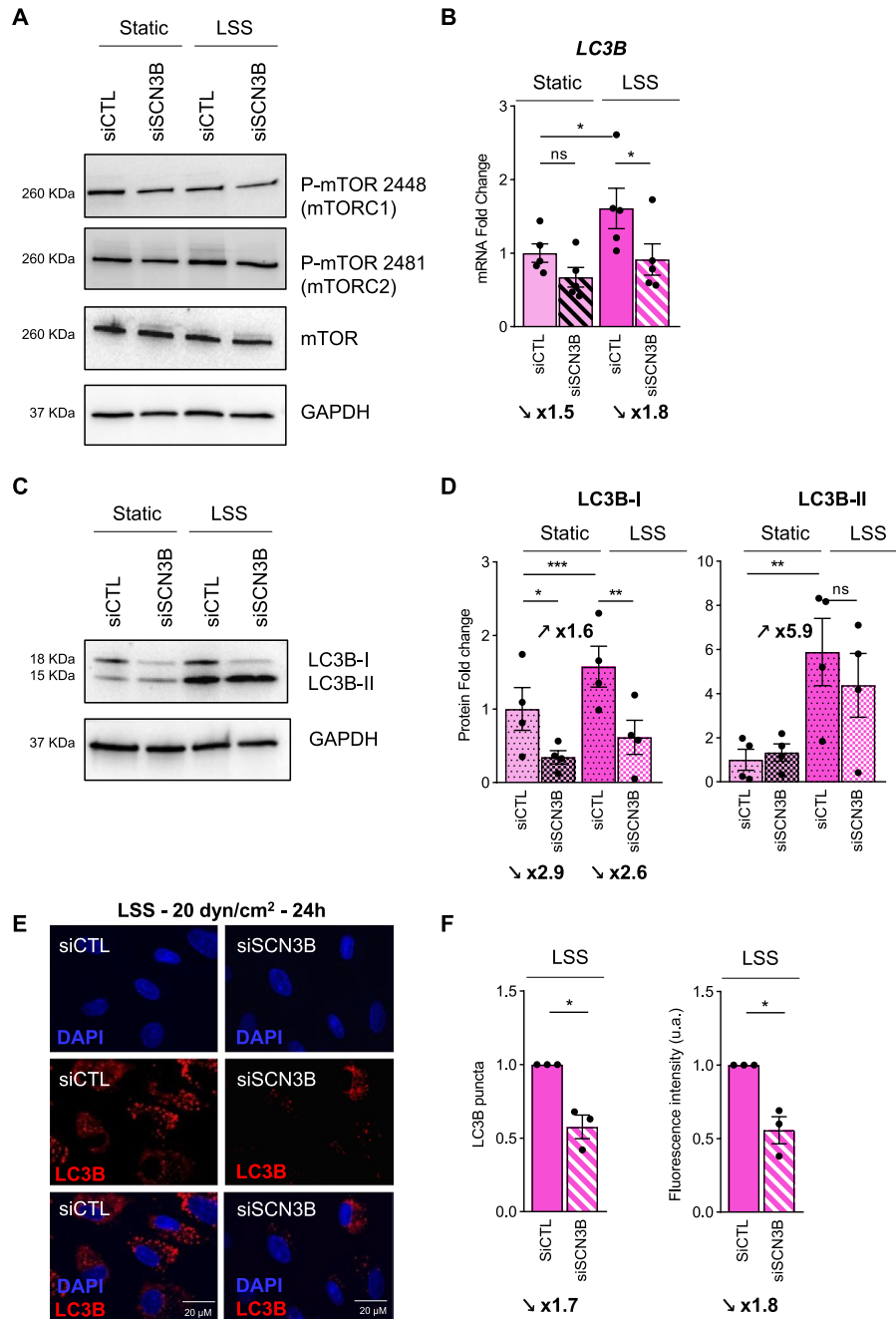


FIGURE 7 | $\text{Na}_v\beta 3$ modulates LC3B expression in TeloHAEC. (A) Protein expression of P-mTOR at serine 2448 (mTORC1 complex) or at serine 2481 (mTORC2 complex) and mTOR in static or LSS (20 dyn/cm²-24h) conditions in TeloHAEC transfected with SiRNA Control (siCTL) or SiRNA targeting SCN3B (siSCN3B). The expression of proteins was evaluated by western blot where ten μg of cell protein extracts were loaded on 4%-20% SDS-PAGE and where GAPDH protein was used as a loading control. (B) mRNA expression of *LC3B* in the same conditions. (C) LC3B protein expression in static or LSS (20 dyn/cm²-24h) conditions in TeloHAEC transfected with SiRNA Control (siCTL) or SiRNA targeting SCN3B (siSCN3B). (D) Densitometry analysis following western blot of the LC3B-I and LC3B-II bands in static and LSS with or without siSCN3B in TeloHAEC. Values of fold change (mRNA and protein) are expressed as mean \pm SEM for at least 4 or 5 independent experiments and compared to static condition, given the arbitrary value of 1 using the $2^{-\Delta\Delta\text{Cq}}$ method for RT-qPCR experiments or normalized to GAPDH for western blot experiments. One-way ANOVA was performed. ns, nonsignificant, * $p < 0.05$, ** $p < 0.01$, *** $p < 0.001$. (E) Representative immunofluorescence images of LC3B staining (red) in TeloHAEC transfected with siCTL or siSCN3B and cultivated under LSS (20 dyn/cm² for 24h). Nuclei (blue) were stained with DAPI. (F) Histograms represent the number of puncta (left) and fluorescence intensity (right) of LC3B staining. Data are presented as mean \pm SEM ($n = 3$) and normalized to siCTL, given the arbitrary value of 1. Significance was analyzed using one sample *t*-test and Wilcoxon test, * $p < 0.05$.

and alignment in the flow direction [10]. We first showed that the immortalized human aortic endothelial cells TeloHAEC behaved as the classical EC model HUVEC, showing

elongation and alignment under LSS. These morphological modifications are accompanied by activation of atheroprotective signaling pathways, that is, KLF2/KLF4/NOS3 induction

A

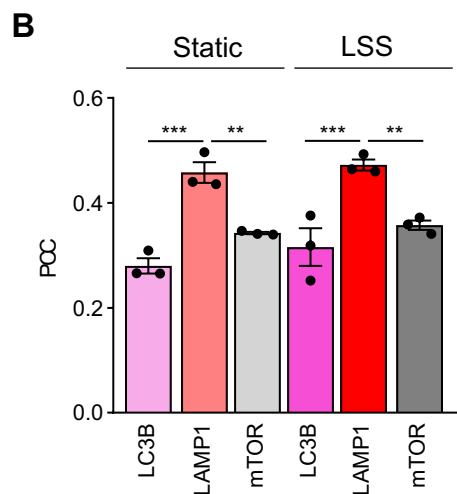
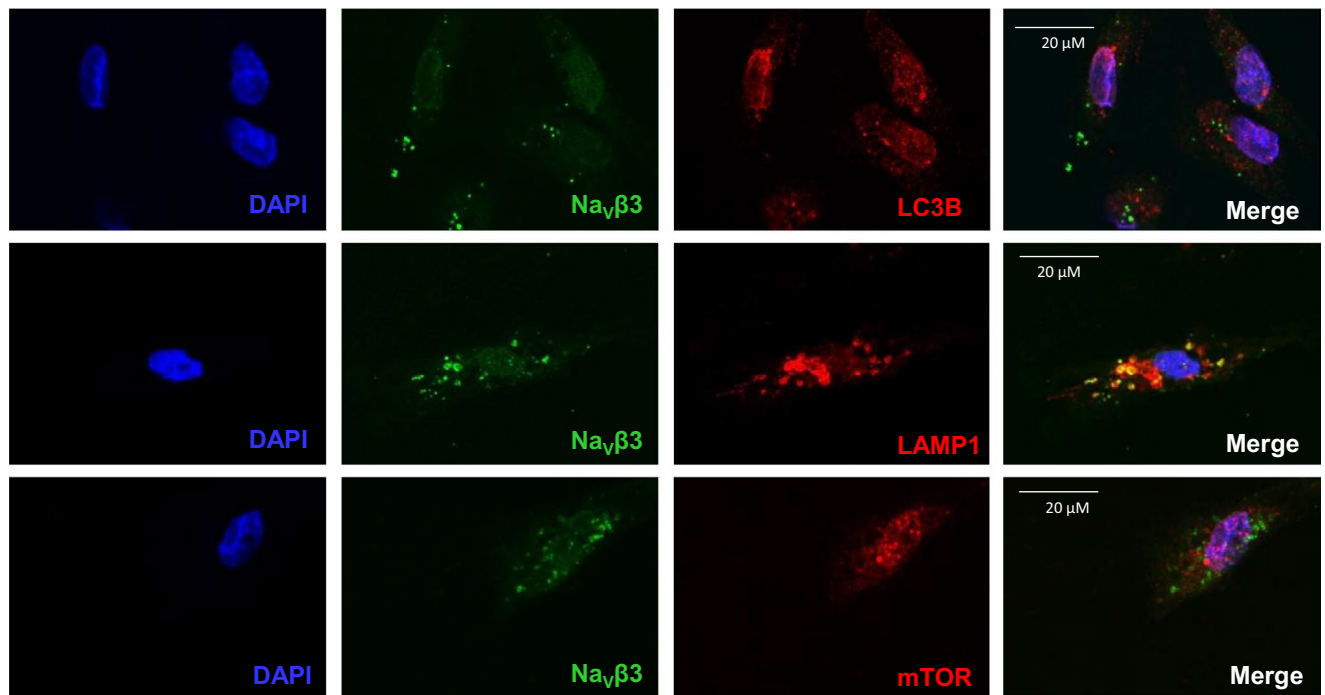


FIGURE 8 | $\text{Na}_v\beta 3$ partially colocalizes with LC3B, LAMP1, and mTOR in TeloHAEC under static or LSS conditions. (A) Representative images illustrating the immunostaining of LC3B, LAMP1 or mTOR (red) together with $\text{Na}_v\beta 3$ (green) in TeloHAEC which were transfected with pmyc-SCN3B and cultivated under static condition. Nuclei (blue) were stained with DAPI. (B) Quantification of the colocalization of $\text{Na}_v\beta 3$ with LC3B, LAMP1 or mTOR was calculated using Pearson's correlation coefficient (PCC). Histogram bars represent the PCC value as mean \pm SEM for each protein (LC3B, LAMP1 or mTOR) in TeloHAEC cultivated under static or LSS conditions for three independent experiments. Significance was analyzed using one-way ANOVA statistical analysis, followed by Tukey multiple comparisons test. ** $p < 0.01$, *** $p < 0.001$.

in TeloHAEC, as previously shown in HUVEC [5, 11]. We then used TeloHAEC since they originate from human aorta, a type of artery prone to atherosclerosis [34, 35]. Therefore, TeloHAEC represent an interesting new model for the investigation of endothelial signaling pathway induced by shear stress.

Among endothelial mechanosensitive ion channels, Na_v channels have emerged as interesting candidates since they are involved in flow-mediated vasodilation in resistance arteries

[18–20, 38]. In this study, we found that TeloHAEC endogenously express $\text{Na}_v1.5$, $\text{Na}_v1.6$, $\text{Na}_v\beta 1$ and $\text{Na}_v\beta 3$, similarly to HUVEC. These data are in agreement with Andrikopoulos' study [20] in which *SCN5A*, *SCN8A*, *SCN9A*, *SCN1B*, and *SCN3B* expression has been reported in HUVEC, at similar levels to our RT-qPCR data obtained in TeloHAEC. The expression of Na_v channel subunits in HUVEC has raised the idea of their noncanonical roles, that is, nonelectrogenic function, such as their contributions to the response of EC to shear stress [21].

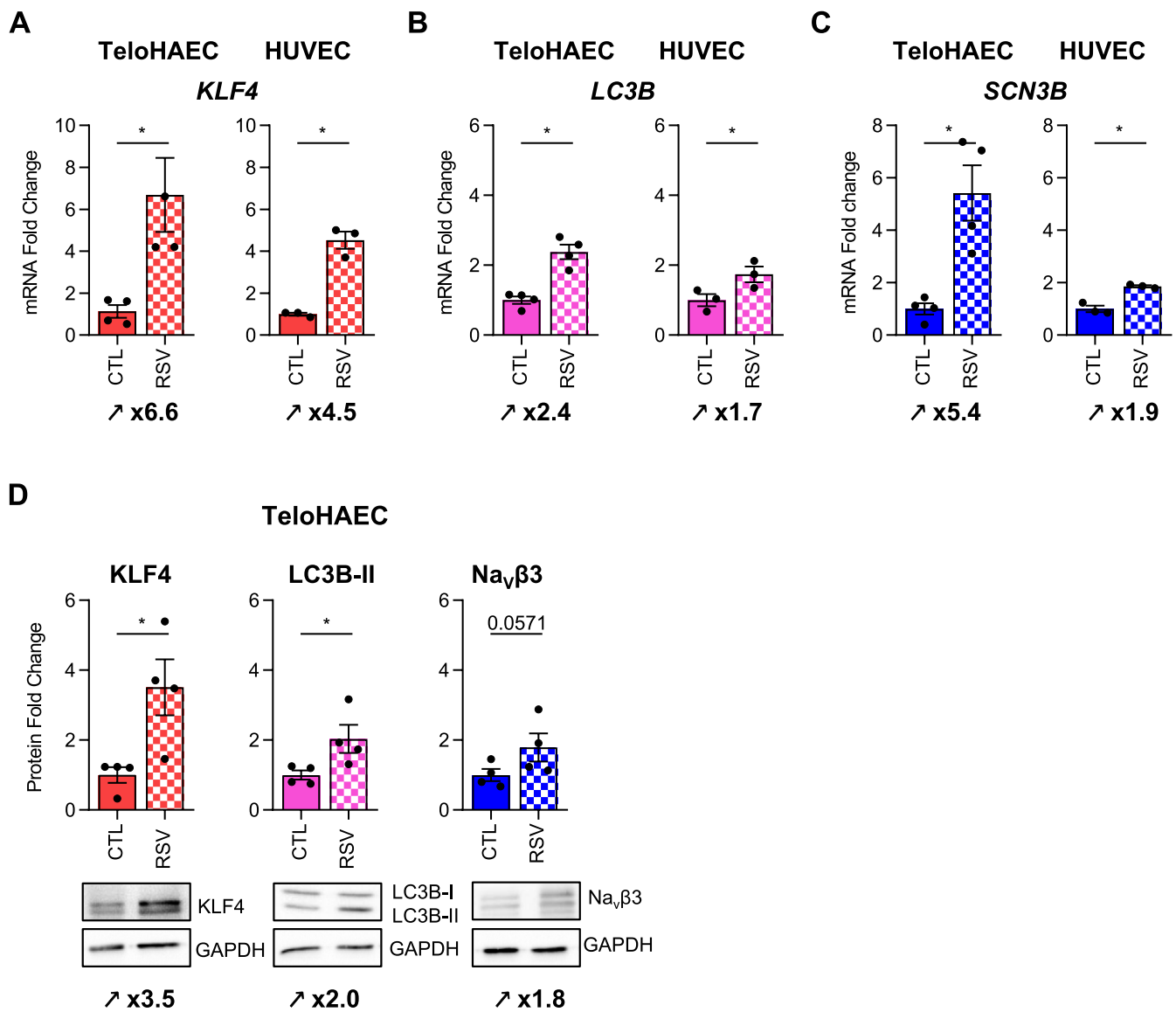


FIGURE 9 | Resveratrol induces *KLF4*, *LC3B*, and *SCN3B* mRNA expression in both TeloHAEC and HUVEC and in *KLF4*, *LC3B*, and *Na_vβ3* protein in TeloHAEC. (A–C) The effects of RSV were evaluated on the expression of *KLF4* (A), *LC3B* (B), and *SCN3B* (C) mRNA in TeloHAEC and HUVEC. (D) The effect of resveratrol was assessed on *KLF4*, *LC3B* and *Na_vβ3* protein expression in TeloHAEC. (A–D) The cells were treated with 100 μM of RSV and 0.1% DMSO (CTL) as negative control. The histogram bars illustrate the fold change values (mRNA and protein) as mean ± SEM ($n=3-4$), compared to CTL, given the arbitrary value of 1 for RT-qPCR data using the $2^{-\Delta\Delta C_q}$ method or normalized to GAPDH (loading control protein) and compared to CTL, given the arbitrary value of 1 for western blotting. Nonparametric unpaired Mann–Whitney tests were performed, $*p<0.05$.

We then found that LSS downregulates *SCN5A* expression. This downregulation could be due to the activation of the transcription factor FoxO1, known to be activated by LSS [39] and to directly repress *SCN5A* transcription. In HUVEC, the inhibition of *Na_v1.5* activity has been shown to decrease cell proliferation [18]; as such, the repression of *SCN5A* expression by LSS might be associated with the reduction in EC proliferation, which occurs under LSS [11].

Our main findings underlying that LSS induces *Na_vβ3* are in agreement with a previous report in GSE datasets, showing that high shear stress leads to *SCN3B* mRNA induction (GSE23289) [44]. Moreover, our data show that the increase of *SCN3B* transcription is mediated by *KLF4* activation since *KLF4*

overexpression induces *Na_vβ3* expression, while the repression of *KLF4* expression decreases *SCN3B* expression under flow. This finding is in accordance with transcriptomic analysis of HUVEC overexpressing *KLF4* (GSE90982), showing that *KLF4* induces an upregulation of *SCN3B* expression [45]. The induction of *SCN3B* could also be mediated by *KLF2*. Indeed, *KLF4* and *KLF2* share many target genes in common, such as *NOS3* [46] due to the similarity of the consensus sequences between *KLF4* and *KLF2*. However, the prediction of response elements for *KLF4* in the *SCN3B* gene exhibits much higher scores than those for *KLF2*. Furthermore, *SCN3B* mRNA is not upregulated in HUVEC infected with *KLF2* lentivirus (GSE19412) [9] nor with *KLF2* adenovirus [6]. In addition, other transcription factors might be involved in *SCN3B* upregulation under shear

stress, such as FoxO1 [47] and p53 transcription factors [48]. Interestingly, both transcription factors have been highlighted as key activators of atheroprotective signaling pathways, as KLF4 [11].

Our data show that *SCN3B* downregulation impairs EC elongation and alignment in response to LSS in TeloHAEC. Other proteins belonging to the Ig-CAM family, including $\text{Na}_v\beta_3$, such as VE-Cadherin or PECAM1 (platelet endothelial cell adhesion molecule), have also been shown to be involved in EC alignment under flow [49, 50]. Additionally, the identification of the protein partners using proteomic analysis demonstrated that $\text{Na}_v\beta_3$ is a partner of mTOR, a negative regulator of autophagy, particularly upon cellular stress such as serum starvation [51]. Of note, autophagy is essential to EC alignment [13–16, 37]. mTOR protein or its phosphorylation is not modulated by LSS, since LSS does not directly modulate or block the mTOR signaling pathway [37]. Thus, we assume that the binding of mTOR to $\text{Na}_v\beta_3$ leads to its sequestration and, in turn, allows the activation of autophagy by increasing autophagosome formation and LC3B expression and subsequently EC alignment. Nevertheless, it remains to determine how $\text{Na}_v\beta_3$ interacts with mTOR. It has been shown that mTOR kinase activity can be inhibited after direct interaction with FKBP12 (FK506-binding protein 12) [51]. This result led us to hypothesize that $\text{Na}_v\beta_3$ could bind mTOR to the same site as FKBP12, leading to the inhibition of mTOR activity. Interestingly, we found that $\text{Na}_v\beta_3$ partially colocalized with mTOR, in accordance with our co-immunoprecipitation results and the idea that $\text{Na}_v\beta_3$ could inhibit mTOR activity by direct interaction and subsequently increase the autophagic flux.

As an auxiliary subunit of Na_v channels belonging to the Ig-CAM family, $\text{Na}_v\beta_3$ is expected to be inserted into the plasma membrane [52]. However, we demonstrated that $\text{Na}_v\beta_3$ is retained in subcellular compartments, mainly in lysosomes and to a lesser extent in autophagosomes and bound mTOR, which is known to be localized to the lysosomes [53]. The localization of $\text{Na}_v\beta_3$ is consistent with recent results concerning another Na_v channel β -subunit isoform, $\text{Na}_v\beta_1$, which is expressed in the endoplasmic reticulum and endolysosomal vesicles [54]. Finally, the gene ontology-term enrichment analysis highlights that several $\text{Na}_v\beta_3$ interactants belong to (i) cellular component of organelle compartment and (ii) biological process related to endomembrane system organization including TMED9 or EI24, both transmembrane proteins associated with autophagy [55, 56], emphasizing the new concept that $\text{Na}_v\beta_3$ is expressed in organelles and particularly in vesicles. Taken together, we propose $\text{Na}_v\beta_3$, expressed at the level of lysosomes, autophagosomes, or autolysosomes, as a novel actor of endothelial autophagy that blocks mTOR function through direct interaction.

Our data highlight the role of Na_v channels in the mechanosignaling pathway, induced by shear stress. In TeloHAEC and HUVEC, $\text{Na}_v1.5$ and $\text{Na}_v\beta_3$ expressions are modulated by LSS, suggesting their contribution as mechanosensors. Indeed, it has been shown that $\text{Na}_v\beta_1$ and $\text{Na}_v\beta_3$ modulate the mechanosensitivity of $\text{Na}_v1.5$ [28]. However, the fact that KLF4 silencing almost totally suppresses *SCN3B* induction in response to shear stress, suggest that $\text{Na}_v\beta_3$ is not directly a mechanosensor such as Piezo1 [57], but rather a downstream actor of the

mechanosignaling pathway. Furthermore, it could be interesting to explore the relationship between $\text{Na}_v\beta_3$ and $\text{Na}_v1.5$ in EC under LSS and the contribution of the resulting Na_v channel complex to membrane potential, Ca^{2+} homeostasis and endothelial function. Since *SCN3B* pathogenic variants are responsible of arrhythmia [58], it would be very interesting to investigate their impact on shear stress response, and other endothelium function such as flow-mediated dilation, that involves autophagic flux [18] or vasculoprotection since $\text{Na}_v\beta_3$ expression is increased by the atheroprotective resveratrol.

In conclusion, this study highlights a novel role of $\text{Na}_v\beta_3$ as a novel intracellular actor of endothelial mechanosignaling, involved in the autophagy pathway through mTOR interaction, which is crucial to cell alignment under shear stress and must contribute to vasculoprotection by increased autophagic flow.

Author Contributions

Claire Legendre conceived and designed the research, performed the experiments, and acquired, analyzed, and interpreted the data, obtained grants, wrote, and edited the manuscript. Christian Legros conceived and designed the research, contributed to the discussion, and critically reviewed the manuscript. Léa Réthoré, Anne-Laure Guihot, Linda Grimaud, Coraline Proux, Alice Boissard, Cécile Henry, Jérôme Cayon, Rodolphe Perrot, Benjamin Barré, François Guillonneau, and Catherine Guette performed the experiments and acquired, analyzed, and interpreted the data. Daniel Henrion contributed to the discussion and reviewed the manuscript. All authors have approved the final version of the manuscript.

Acknowledgments

The authors are grateful to Louis Gourdin (MITOVASC, Equipe CarME, University of Angers) for his technical help.

Conflicts of Interest

The authors declare no conflicts of interest.

Data Availability Statement

The data that support the findings of this study are available in the article and/or [Supporting Information](#) tables. Additional data supporting the findings of this study may be requested from the corresponding author.

References

1. J. E. Deanfield, J. P. Halcox, and T. J. Rabelink, “Endothelial Function and Dysfunction: Testing and Clinical Relevance,” *Circulation* 115 (2007): 1285–1295.
2. N. Baeyens, C. Bandyopadhyay, B. G. Coon, S. Yun, and M. A. Schwartz, “Endothelial Fluid Shear Stress Sensing in Vascular Health and Disease,” *Journal of Clinical Investigation* 126 (2016): 821–828.
3. M. J. Davis, S. Earley, Y.-S. Li, and S. Chien, “Vascular Mechanotransduction,” *Physiological Reviews* 103 (2023): 1247–1421.
4. S. Chatterjee, “Endothelial Mechanotransduction, Redox Signaling and the Regulation of Vascular Inflammatory Pathways,” *Frontiers in Physiology* 9 (2018): 524.
5. M. R. Maurya, S. Gupta, J. Y.-S. Li, et al., “Longitudinal Shear Stress Response in Human Endothelial Cells to Atheroprone and Atheroprotective Conditions,” *Proceedings of the National Academy of Sciences of the United States of America* 118 (2021): e2023236118.

6. K. M. Parmar, "Integration of Flow-Dependent Endothelial Phenotypes by Kruppel-Like Factor 2," *Journal of Clinical Investigation* 116, no. 1 (2005): 49–58.
7. L. V. Dekker, Z. Daniels, C. Hick, et al., "Analysis of Human Nav1.8 Expressed in SH-SY5Y Neuroblastoma Cells," *European Journal of Pharmacology* 528 (2005): 52–58.
8. A. Hamik, Z. Lin, A. Kumar, et al., "Kruppel-Like Factor 4 Regulates Endothelial Inflammation," *Journal of Biological Chemistry* 282 (2007): 13769–13779.
9. R. A. Boon, T. A. Leyen, R. D. Fontijn, et al., "KLF2-Induced Actin Shear Fibers Control Both Alignment to Flow and JNK Signaling in Vascular Endothelium," *Blood* 115 (2010): 2533–2542.
10. J. Kroon, N. Heemskerk, M. J. T. Kalsbeek, V. de Waard, J. van Rijssel, and J. D. van Buul, "Flow-Induced Endothelial Cell Alignment Requires the RhoGEF Trio as a Scaffold Protein to Polarize Active Rac1 Distribution," *Molecular Biology of the Cell* 28 (2017): 1745–1753.
11. H. Nakajima and N. Mochizuki, "Flow Pattern-Dependent Endothelial Cell Responses Through Transcriptional Regulation," *Cell Cycle* 16 (2017): 1893–1901.
12. G. R. Y. De Meyer, M. O. J. Grootaert, C. F. Michiels, A. Kurdi, D. M. Schrijvers, and W. Martinet, "Autophagy in Vascular Disease," *Circulation Research* 116 (2015): 468–479.
13. S.-K. Park, D. T. La Salle, J. Cerbie, et al., "Elevated Arterial Shear Rate Increases Indexes of Endothelial Cell Autophagy and Nitric Oxide Synthase Activation in Humans," *American Journal of Physiology—Heart and Circulatory Physiology* 316 (2019): H106–H112.
14. Q. Meng, L. Pu, M. Qi, et al., "Laminar Shear Stress Inhibits Inflammation by Activating Autophagy in Human Aortic Endothelial Cells Through HMGB1 Nuclear Translocation," *Communications Biology* 5 (2022): 425.
15. A.-C. Vion, M. Kheloufi, A. Hammoutene, et al., "Autophagy Is Required for Endothelial Cell Alignment and Atheroprotection Under Physiological Blood Flow," *Proceedings of the National Academy of Sciences of the United States of America* 114 (2017): E8675–E8684.
16. M. Chen, L. Yi, X. Jin, et al., "Resveratrol Attenuates Vascular Endothelial Inflammation by Inducing Autophagy Through the cAMP Signaling Pathway," *Autophagy* 9 (2013): 2033–2045.
17. X. Zhou, J. Yang, M. Zhou, et al., "Resveratrol Attenuates Endothelial Oxidative Injury by Inducing Autophagy via the Activation of Transcription Factor EB," *Nutrition & Metabolism (London)* 16 (2019): 42.
18. P. Nivoit, T. Mathivet, J. Wu, et al., "Autophagy Protein 5 Controls Flow-Dependent Endothelial Functions," *Cellular and Molecular Life Sciences* 80 (2023): 210.
19. K. A. Gerhold and M. A. Schwartz, "Ion Channels in Endothelial Responses to Fluid Shear Stress," *Physiology* 31 (2016): 359–369.
20. P. Andrikopoulos, S. P. Fraser, L. Patterson, et al., "Angiogenic Functions of Voltage-Gated Na⁺ Channels in Human Endothelial Cells: Modulation of Vascular Endothelial Growth Factor (VEGF) Signaling," *Journal of Biological Chemistry* 286 (2011): 16846–16860.
21. O. Traub, T. Ishida, M. Ishida, J. C. Tupper, and B. C. Berk, "Shear Stress-Mediated Extracellular Signal-Regulated Kinase Activation Is Regulated by Sodium in Endothelial Cells. Potential Role for a Voltage-Dependent Sodium Channel," *Journal of Biological Chemistry* 274 (1999): 20144–20150.
22. J. Park, C. Proux, W. Ehanho, et al., "Tetrodotoxin Decreases the Contractility of Mesenteric Arteries, Revealing the Contribution of Voltage-Gated Na⁺ Channels in Vascular Tone Regulation," *Marine Drugs* 21 (2023): 196.
23. W. A. Catterall, "Voltage-Gated Sodium Channels at 60: Structure, Function and Pathophysiology," *Journal of Physiology* 590 (2012): 2577–2589.
24. J. A. Black and S. G. Waxman, "Noncanonical Roles of Voltage-Gated Sodium Channels," *Neuron* 80 (2013): 280–291.
25. L. M. Carrithers, P. Hulseberg, M. Sandor, and M. D. Carrithers, "The Human Macrophage Sodium Channel Nav1.5 Regulates Mycobacteria Processing Through Organelle Polarization and Localized Calcium Oscillations," *FEMS Immunology and Medical Microbiology* 63 (2011): 319–327.
26. S. Roger, L. Gillet, J.-Y. Le Guennec, and P. Besson, "Voltage-Gated Sodium Channels and Cancer: Is Excitability Their Primary Role?," *Frontiers in Pharmacology* 6 (2015): 152.
27. C. E. Morris, "Voltage-Gated Channel Mechanosensitivity: Fact or Friction?," *Frontiers in Physiology* 2 (2011): 25.
28. M. Maroni, J. Körner, J. Schüttler, B. Winner, A. Lampert, and E. Eberhardt, "β1 and β3 Subunits Amplify Mechanosensitivity of the Cardiac Voltage-Gated Sodium Channel Nav1.5," *Pflügers Archiv—European Journal of Physiology* 471 (2019): 1481–1492.
29. A. Beyder, P. R. Strege, S. Reyes, et al., "Ranolazine Decreases Mechanosensitivity of the Voltage-Gated Sodium Ion Channel Na V 1.5: A Novel Mechanism of Drug Action," *Circulation* 125 (2012): 2698–2706.
30. J. Körner, J. Meents, J.-P. Machtens, and A. Lampert, "β1 Subunit Stabilises Sodium Channel Nav1.7 Against Mechanical Stress: Nav β1 Subunit as Mechanical Stabiliser," *Journal of Physiology* 596 (2018): 2433–2445.
31. P. R. Strege, A. Mercado-Perez, A. Mazzone, et al., "SCN5A Mutation G615E Results in Nav1.5 Voltage-Gated Sodium Channels With Normal Voltage-Dependent Function Yet Loss of Mechanosensitivity," *Channels (Austin, Tex.)* 13, no. 1 (2019): 287–298.
32. dMIQE Group and J. F. Huggett, "The Digital MIQE Guidelines Update: Minimum Information for Publication of Quantitative Digital PCR Experiments for 2020," *Clinical Chemistry* 66 (2020): 1012–1029.
33. S. A. Bustin, V. Benes, J. A. Garson, et al., "The MIQE Guidelines: Minimum Information for Publication of Quantitative Real-Time PCR Experiments," *Clinical Chemistry* 55 (2009): 611–622.
34. M. D. Krause, R.-T. Huang, D. Wu, et al., "Genetic Variant at Coronary Artery Disease and Ischemic Stroke Locus 1p32.2 Regulates Endothelial Responses to Hemodynamics," *Proceedings of the National Academy of Sciences of the United States of America* 115 (2018): E11349–E11358.
35. N. D'Onofrio, C. Sardu, M. C. Trotta, et al., "Sodium-Glucose Co-Transporter2 Expression and Inflammatory Activity in Diabetic Atherosclerotic Plaques: Effects of Sodium-Glucose Co-Transporter2 Inhibitor Treatment," *Molecular Metabolism* 54 (2021): 101337.
36. J. Abello, S. Raghavan, Y. Y. Yien, and A. N. Stratman, "Peristaltic Pumps Adapted for Laminar Flow Experiments Enhance In Vitro Modeling of Vascular Cell Behavior," *Journal of Biological Chemistry* 298 (2022): 102404.
37. V. Mastelj, C. Axen, A. Wary, R. D. Minshall, and K. K. Wary, "A Requirement for Krüppel Like Factor-4 in the Maintenance of Endothelial Cell Quiescence," *Frontiers in Cell and Developmental Biology* 10 (2022): 1003028.
38. S. C. Taylor, G. Laperriere, and H. Germain, "Droplet Digital PCR Versus qPCR for Gene Expression Analysis With Low Abundant Targets: From Variable Nonsense to Publication Quality Data," *Scientific Reports* 7 (2017): 2409.
39. J. Liu, X. Bi, T. Chen, et al., "Shear Stress Regulates Endothelial Cell Autophagy via Redox Regulation and Sirt1 Expression," *Cell Death & Disease* 6 (2015): e1827.
40. C. L. Oeste, E. Seco, W. F. Patton, P. Boya, and D. Pérez-Sala, "Interactions Between Autophagic and Endo-Lysosomal Markers in Endothelial Cells," *Histochemistry and Cell Biology* 139 (2013): 659–670.

41. H. Berrougui, G. Grenier, S. Loued, G. Drouin, and A. Khalil, "A New Insight Into Resveratrol as an Atheroprotective Compound: Inhibition of Lipid Peroxidation and Enhancement of Cholesterol Efflux," *Atherosclerosis* 207 (2009): 420–427.
42. G. Villarreal, Y. Zhang, H. B. Larman, J. Gracia-Sancho, A. Koo, and G. Garcia-Cardena, "Defining the Regulation of Klf4 Expression and Its Downstream Transcriptional Targets in Vascular Endothelial Cells," *Biochemical and Biophysical Research Communications* 391, no. 1 (2010): 984–989.
43. X. F. Figueroa, C.-C. Chen, K. P. Campbell, et al., "Are Voltage-Dependent Ion Channels Involved in the Endothelial Cell Control of Vasomotor Tone?," *American Journal of Physiology. Heart and Circulatory Physiology* 293 (2007): H1371–H1383.
44. S. J. White, E. M. Hayes, S. Lehoux, J. Y. Jeremy, A. J. Horrevoets, and A. C. Newby, "Characterization of the Differential Response of Endothelial Cells Exposed to Normal and Elevated Laminar Shear Stress," *Journal of Cellular Physiology* 226, no. 11 (2011): 2841–2848.
45. Z. Li, M. Martin, J. Zhang, et al., "KLF4 Regulation of Ch25h and LXR Mitigates Atherosclerosis Susceptibility," *Circulation* 136 (2017): 1315–1330.
46. G. Zhou, A. Hamik, L. Nayak, et al., "Endothelial Kruppel-Like Factor 4 Protects Against Atherothrombosis in Mice," *Journal of Clinical Investigation* 122 (2012): 4727–4731.
47. B. Cai, N. Wang, W. Mao, et al., "Deletion of FoxO1 Leads to Shortening of QRS by Increasing Na⁺ Channel Activity Through Enhanced Expression of Both Cardiac NaV1.5 and β 3 Subunit," *Journal of Molecular and Cellular Cardiology* 74 (2014): 297–306.
48. K. Adachi, M. Toyota, Y. Sasaki, et al., "Identification of SCN3B as a Novel p53-Inducible Proapoptotic Gene," *Oncogene* 23 (2004): 7791–7798.
49. E. Chuntharpursat-Bon, O. V. Povstyan, M. J. Ludlow, et al., "PIEZO1 and PECAM1 Interact at Cell-Cell Junctions and Partner in Endothelial Force Sensing," *Communications Biology* 6 (2023): 1–18.
50. D. E. Conway and M. A. Schwartz, "Mechanotransduction of Shear Stress Occurs Through Changes in VE-Cadherin and PECAM-1 Tension: Implications for Cell Migration," *Cell Adhesion & Migration* 9 (2015): 335–339.
51. Y. C. Kim and K.-L. Guan, "mTOR: A Pharmacologic Target for Autophagy Regulation," *Journal of Clinical Investigation* 125 (2015): 25–32.
52. S. Namadurai, N. R. Yerreddi, F. S. Cusdin, C. L.-H. Huang, D. Y. Chirgadze, and A. P. Jackson, "A New Look at Sodium Channel β Subunits," *Open Biology* 5 (2015): 140192.
53. C. Betz and M. N. Hall, "Where Is mTOR and What Is It Doing There?," *Journal of Cell Biology* 203 (2013): 563–574.
54. A. S. Haworth, S. L. Hodges, A. L. Capatina, L. L. Isom, C. G. Bauermann, and W. J. Brackenbury, "Subcellular Dynamics and Functional Activity of the Cleaved Intracellular Domain of the Na⁺ Channel β 1 Subunit," *Journal of Biological Chemistry* 298 (2022): 102174.
55. S. Li, R. Yan, J. Xu, et al., "A New Type of ERGIC–ERES Membrane Contact Mediated by TMED9 and SEC12 Is Required for Autophagosome Biogenesis," *Cell Research* 32 (2022): 119–138.
56. S. Devkota, H. Jeong, Y. Kim, et al., "Functional Characterization of EI24-Induced Autophagy in the Degradation of RING-Domain E3 Ligases," *Autophagy* 12 (2016): 2038–2053.
57. M. B. Goodman, E. S. Haswell, and V. Vásquez, "Mechanosensitive Membrane Proteins: Usual and Unusual Suspects in Mediating Mechanotransduction," *Journal of General Physiology* 155, no. 3 (2023): e202213248.
58. H. A. O'Malley and L. L. Isom, "Sodium Channel β Subunits: Emerging Targets in Channelopathies," *Annual Review of Physiology* 77 (2015): 481–504.

Supporting Information

Additional supporting information can be found online in the Supporting Information section.